TOMOGRAPHIC IMAGING OF IONOSPHERIC ELECTRON DENSITY OVER EASTERN AFRICA USING MULTI-PLATFORM INSTRUMENTATIONS AND MODEL IONOSPHERIC TOTAL ELECTRON CONTENT

By
Asmelash Gebremedihn

SUBMITTED IN PARTIAL FULFILLMENT OF THE
REQUIREMENTS FOR THE DEGREE OF
MASTER OF SCIENCE
IN PHYSICS (SPACE PHYSICS)
AT
ADDIS ABABA UNIVERSITY
ADDIS ABABA, ETHIOPIA
JUNE 28, 2013

Copyright © Asmelash Gebremedihn 2013

All Rights Reserved

ADDIS ABABA UNIVERSITY
DEPARTMENT OF PHYSICS

Dated: JUNE 28, 2013

THE UNDERSIGNED HEREBY CERTIFY THAT THEY HAVE READ AND RECOMMEND TO THE COLLEGE OF GRADUATE STUDIES FOR ACCEPTANCE A THESIS ENTITLED "**Tomographic imaging of ionospheric electron density over Eastern Africa using multi-platform instrumentations and model ionospheric total electron content** " BY **ASMELASH GEBREMEDIHN** IN PARTIAL FULFILLMENT OF THE REQUIREMENTS FOR THE DEGREE OF **MASTER OF SCIENCE.**

SUPERVISOR: _____
Dr. GIZAW MENGISTU

EXAMINERS: _____
Prof. A.V. Gholap

_____
Dr. Kassahun Ture

ADDIS ABABA UNIVERSITY

Date: **June 28, 2013**

Author: **Asmelash Gebremedihn**

Title: **Tomographic imaging of ionospheric electron density over Eastern Africa using multi-platform instrumentations and model ionospheric total electron content**

Department: **PHYSICS**

Degree: **M.Sc.** Convocation: **JUNE** Year: **2013**

PERMISSION IS HEREWITH GRANTED TO ADDIS ABABA UNIVERSITY TO CIRCULATE AND TO HAVE COPIED FOR NON-COMMERCIAL PURPOSES, AT ITS DISCRETION, THE ABOVE TITLE UPON THE REQUEST OF INDIVIDUALS OR INSTITUTIONS.

_____

Signature of Author

THE AUTHOR RESERVES OTHER PUBLICATION RIGHTS, AND NEITHER THE THESIS NOR EXTENSIVE EXTRACTS FROM IT MAY BE PRINTED OR OTHERWISE REPRODUCED WITHOUT THE AUTHOR'S WRITTEN PERMISSION.

THE AUTHOR ATTESTS THAT PERMISSION HAS BEEN OBTAINED FOR THE USE OF ANY COPYRIGHTED MATERIAL APPEARING IN THIS THESIS (OTHER THAN BRIEF EXCERPTS REQUIRING ONLY PROPER ACKNOWLEDGEMENT IN SCHOLARLY WRITING) AND THAT ALL SUCH USE IS CLEARLY ACKNOWLEDGED.

Abstract

A 3D - computerized tomography technique has been used to investigate the electron density of the low - latitude ionosphere during the low solar minimum in 2008 over the East Africa region. The 3D - tomography uses Damped Least Square inversion with the second order Tikhonove Regularization (DLSTR) algorithm. The TEC used in the tomographic inversion is obtained from the observables measured by a chain of station reciving transit satellite transmission over the region. The algorithm employes electron density from NeQuick model as apriori values. The electron density obtained from the inversion is a weighted combination of the apriori electron density and that obtaind from GPS measurement. The results show that the reconstructed electron density exhibits the required diurnal, latitudinal and longitudinal variations consistent with the physics of plasma formation and transport.

Acknowledgements

This research would not have been possible without the support of many people. First of all, I am deeply indebted to my advisor Dr. Gizaw Mengistu for his passionate and unreserved support during this research. Dr. Gizaw Mengistu is a hard work and self confident always helpful makes me in the right track and I learned a lot, indeed. The data used in this work is generated by a matlab code developed by Mengistu Tsidu (2012) for use of various data from multiple instrumentts to retrieve ionospheric electron density using tomographic techniques. I am also thankful to all the department members.
Ofcourse, I am grateful to my aunt W/z Zemeda Hagos and her son Hintsa weldegebriel and love. Without W/z Zemeda Hagos and Hintsa weldegebriel this work would never have come into existence (literally).
I would like to thank to my father and Abudu Abdelkadr for their support and encourage for all good and bad times I had.
Finally, I wish to thank the following: Haji juhar and his family, Eido Shemeni, Beza Tesfaye, Fikir Tesfaye, Jemal Seid and for all the good and bad times we had together.

Contents

List of Figures

List of Acronyms

GPS	Global Positioning System
LEO	Low-Earth-Orbit
TEC	Total Electron Content
STEC	Slant Total Electron Content
CDAAC	COSMIC Data Analysis and Archive Center
RO	Radio Occultation

Introduction

The knowledge of the electron density distribution in the Earth‘s ionosphere and plasmasphere is important for several purposes, such as estimation and correction of propagation delays in the Global Positioning System (GPS); improving the accuracy of satellite navigation; predicting changes due to ionospheric storms; predicting space weather effects on telecommunications, and many more [1]. Information about ionospheric electron density can be derived from a range of different instruments. New opportunities are provided by the Global Positioning System (GPS) satellites. GPS consists of 32 satellites that transmit L-band radio signals at 1.575 and 1.228 GHz. Dual-frequency GPS signals can be recorded at ground-based receivers to obtain the signals relative phase shift and delay. The dispersive nature of the ionospheric component allows the ionospheric delay to be determined separately from effects caused by propagation through the non-ionised part of the atmosphere. This provides information that can be related directly to TEC.
GPS signals are providing an important and inexpensive new tool for ionospheric measurement. The utilisation of such navigation system satellites for ionospheric research has the advantage of being very cost effective; no new satellite is required and the transmissions are at present free to everyone. Moreover, the receivers are commercially available at low cost. However, from any observation site the satellites appear at changing and oblique angles. Consequently the observations of total electron content are each along a different line-of-sight and thus are very complicated to interpret.
The radio-occultation technique uses receivers located on Low-Earth-Orbit (LEO) satellites to monitor the phase changes of GPS signals. These radio-occultation experiments have already been very successful for neutral atmospheric studies. Satellite measurements are now increasingly used for ionospheric work. Hajj et al. (1994) suggested using the satellite-to-satellite transmission of GPS to LEO satellite measurements in a tomographic framework to provide the so-called “missing horizontal rays” and improve the vertical resolution. In addition, LEOs provide measurements over the oceans and into remote polar caps, thus enabling the ionosphere to be studied on a truly global-scale [18].
This thesis is outlined as follows: review of the ionosphere is given in Chapter 1. Chapter 2 discusses COSMIC data and radio occultation technique. Chapter 3 covers ionospheric tomography and algorithm. Result and Analysis are give in Chapter 4. Finally, we give summery and conclusion of our study in Chapter 5.

Chapter 1

The Ionosphere

The term ionosphere was first used by Sir Robert Watson-Watt in a letter to the secretary of the British Radio Research Board. The expression came into wide use during the period 1932-34 when Watson-Watt, Appleton, Ratcliff and others used it in papers and books. Before the term ionosphere gained worldwide acceptance, it was called the Kennelly-Heaviside layer, the upper conducting layer, ionized upper atmosphere [3]. The ionosphere is a region above the surface of Earth that extends from a height of about 50 km to 2,000 km, where solar irradiance produces a partially ionized plasma and the electron concentration is constantly changing as it is illuminated by the sun, pushed by winds, and bombarded by cosmic rays and solar particles. Knowledge of the ionospheric electron density is essential for a wide range of applications, e.g., radio and telecommunicati-ons, satellite tracking and Earth observation from space. In some cases, the ionosphere is necessary (for example, short wave broadcasts and over the horizon radar), and in other cases the ionosphere hinders radio wave propagation (for example, communications and navigation satellite signals).
Electron density concentration varies with height or distance from the earth's surface, latitude, time of day, season, and amount of solar activity. Regions of irregularity also exist and may range in size from less than a meter to hundreds of kilometers. Due to these irregularities, electron concentrations between neighboring regions in the ionosphere may vary up to a factor of 1000 within a distance of just a few kilometers. At present, imaging the electron density is the best method of determining the location and nature of these irregularities so that one can accurately determine how signals will be reflected due to variations and irregularities in electron density concentration as they traverse the ionosphere [4].
It is therefore necessary to find a method of imaging the electron distributions in the ionosphere, specifically, of imaging the electron density. Since the ionosphere is not well suited to measurement, several experimental techniques have been developed to measure the densities at specific positions or along specific directions in the ionosphere. The three most widely used techniques for examining the electron density in the ionosphere are ionosonde measurements, incoherent scatter radar, and differential Doppler methods. All this techniques have their own contribution to study ionosphere but in this thesis we are using GPS measurement technique, since there is no other measurements in the area.

1.1 The Earth's Magnetic Field

The earth′s magnetic field plays an important role in the formation of the ionosphere. This highlights the importance of using geomagnetic field coordinates to describe or model of the

ionosphere. The first approximation to the earth′s magnetic field is that of a sphere uniformly magnetized in the direction of the centered dipole axis. This axis cuts the surface of the earth at points known as the austral (south) and boreal (north) dipole poles. The intersection between the plane through the earth center perpendicular to the dipole axis and the earth surface is called the geomagnetic equator. Scientists use dip latitude to describe the earth′s actual magnetic field. In this case, the poles are referred to as dip poles, locations where the geomagnetic field is vertical to the earth′s surface, and dip equator where the geomagnetic field is horizontal. Detailed descriptions of the earth′s magnetic field, and relationships among geographic, geomagnetic, and dip latitudes have been given by several authors [3].

1.2 Structure and composition of the Ionosphere

The ionosphere is the ionized plasma in the atmosphere which is created by photoionization of the neutral atmosphere by extreme ultra violet (EUV) radiation and high energy solar particles [5]. The ionosphere is constituted of free electrons and ions which are produced during interaction of extreme ultra violet (EUV) and X-ray radiation with upper atmosphere neutral gas during ionization, a process involving the stripping of electrons from neutral atoms in the atmosphere to form positively charged ions and negatively charged electrons. The net value of the number of free ions and electrons in the ionosphere is determined by the rate at which specific species of ions recombine with electrons to form neutral atoms, a process called recombination. Two types of recombination are involved:
Radiative recombination:- Electrons combine directly with ions, converting them into neutral atoms and emmitting a photon to conserve energy and momentum, e.g.,

$$O^+ + e^- \rightarrow O + photon \tag{1.1}$$

Dissociative recombination:- is a two-stage process. In the first stage, positive ions (e.g., N^+) interact with neutral molecules (e.g., O_2), replacing one of the atoms in the molecule and forming a neutral atom and a positively charged molecular ion, e.g.

$$NO_2^+ + e^- \rightarrow NO^+ + O \tag{1.2}$$

In the second stage, electrons combine with the newly formed molecular ion, forming two neutral atoms

$$NO^+ + e^- \rightarrow N + O \tag{1.3}$$

The dissociative recombination rate is about 1000 faster than the radiative recombination, resulting in much shorter lifetime for molecular ions than for atomic ions. Due to molecular ions short life span, when their production is rapidly reduced at night, rapid recombination quickly reduces the plasma concentration. The O^+ at higher altitudes often survives the night . Daytime ionization involving UV radiation is termed photoionization. Because different gas atoms and molecules are more abundant in some regions of the neutral atmosphere than others, ionization and recombination of the different species result in differing electron densities concentrated at different layers of the ionosphere. These layers are called the D, E and F regions (Fig. 1.1) and their structure [6].

The D-Region

The D region is the lowest ionosphere layer extends from approximatley 50 to 90 km (therefore it extends down into the mesosphere). In this layer, the primary source of ionization is cosmic

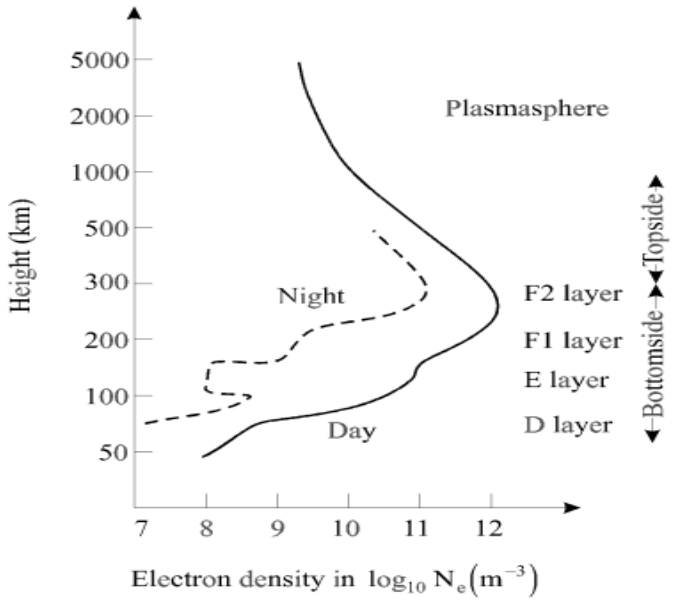

Figure 1.1: Typical vertical profile of the ionosphere (after Davies [1990]).

radiation which is the same by day and by night manifesting itself in a strong solar cycle variation in the D layer electron density. Despite this, by night, the electrons may become attached to atoms and molecules forming negative ions that cause the D layer to disappear. By day, as a consequence of sun′s radiation, the electrons tend to detach themselves from the ions causing the D layer electrons to reappear. As a consequence of that, at the altitude of about 60 to 70 km, the D layer electrons are present by day but not by night causing a distinct diurnal variation in the electron density. Electric charges transfer between different species, and positive and negative ions form complex clusters with water molecules.
The typical values for the noon time electron densities of the D layer at the mid-latitude region range between 6.1×10^8 to 13.1×10^8 electron/m^3 according to the solar activity [3]. The D-region is mainly responsible for HF absorption around 10 MHz and below with smaller absorption at night and greatest at midday [6].

The E-Region

This region is orginally called the kennelly heavy side or just the heavisied layer. It extends from 90 to 120 km and it is essentially a Chapman layer that is formed by the 80 to 102.7 nm part of the EUV spectrum. The main initial ion in this region is O_2^+, with some production of N_2^+ and O^+. The N_2^+ ions are rapidly transformed to other ions by the following reactions:

$$N_2^+ + O \rightarrow NO^+ + N \tag{1.4}$$

$$N_2^+ + O \rightarrow O^+ + N_2 \tag{1.5}$$

while oxygen ions are removed by the following reaction:

$$O^+ + N_2 \rightarrow NO^+ + N \tag{1.6}$$

$$O^+ + O_2 \rightarrow O_2^+ + O \tag{1.7}$$

The end result of these reaction is that the major ions in the day side E region are O^+ and NO^+ (under average conditions the NO^+ concentration of O_2^+). The total ion density or

elecron density profile in the E region layer is basically consistent with Chapman layer [7]. There are other, more transient source of ionozation at E region heights, including complex dynamic resulting from the effect of neutral atmosphere motion, auroral electric fields, and meteors entering the upper atmosphere that oblate (or burn up) and impact the surrounding neutral gas with enough energy to create an ionized trail. These sources produce narrow, short-lived regions of high-density ionization at E region altitudes, known collectively as Sporadic E. The mechanisms responsible for Sporadic E depend on latitude. Sporadic E can last from few minutes to several hours. Ionization can be locally very high, and therefore, high-frequency radio waves can be reflected off these trails for long-distance communication [8].

The F_1-Region

The main source of ionization in the F_1 layer is the EUV light. The F1 layer is only observed during the day since the electron densities are primarily controlled by the zenith angle of the sun. When it is present, it changes rapidly in a matter of minutes. It is more pronounced during the summer than during the winter months for low solar sunspot numbers and for periods with ionospheric storms. Typical noon time mid-latitude electron densities range between 2.3×10^{11} and 3.3×10^{11} electrons/m^3 according to the solar activity [3].
The F_1 region is also essentially a Chapman layer and the ionizing solar flux is in the $<$91 nm EUV spectral region. It is basically obsorbed in this layer and does not penetrate in to the E region. The principal initial ion in the F_1 region is O^+, with some contribution from N_2^+. In the lower F_1 region (around 140 km) the life time of the O^+ is quite short (a few seconds), and therefore the NO^+ molecular ion become dominant. Above approximately 180 km, O^+ rapidly takes over and become the major ion [7].

The F_2-Region

The F_2 layer is the most important ionospheric layer from the point of view of HF propagation. The F_2 layer does not follow the solar zenith angle dependence. In fact, the January noon F_2 layer critical frequency (foF_2) is more than twice the summer value. Interestingly, this winter anomaly occurs in the daytime only which is thought to be due to the large summer electron loss caused by the increased molecular to atomic composition of the neutral atmosphere. In summer, foF_2 shows little diurnal variation. The global spatial distribution of foF_2 reveals a strong geomagnetic dependence. The most distinctive features are the two regions of high foF_2 lying about 20 degrees dip latitude which is called the equatorial anomaly. F_2 layer critical frequencies also show a linear dependence with solar sunspot numbers. Typical mid-latitude noon time electron densities range between 2.8×10^{11} and 5.2×10^{11} electrons/m^3 according to the solar activity [3].
In this region the major ion is O^+ with a density peak in the 200 to 400 km range. This region clearly can not be a Champ layer, since the atmosphere above The F_1 is optically thin to most ionizing radiation. The formation of F_2 peak is caused by an interplay between ion source sinks, and ambipolar diffussion [7].
In the F_2 region the dominant ionization source is the photoionization of atomic oxygen:

$$O + h\nu \rightarrow O^+ + e \tag{1.8}$$

1.3 Chapman Production

Sydney Chapman presented in 1931 a simple mathematical model for the formation of ionized layers, which was based on the fact that energetic photons from the sun split air molecules into electrons and positive ions. The model describes the major characteristics of the observed variations in the different layers of the ionosphere. The goal is to develop a simple model for how the plasma density varies with height and the suns zenith angle (χ). The altitude profile of ion production will have a peak at some altitude, because the rate of some ionization depends on both neutral density (which decrease with height) and the incoming solar-radiation intensity (which increase with height). The presumed to be exponential, planer and horizontally stratified (assumpition that are idealization of the real world, where the atmosphere are only approximately exponential, curved and the scale height H_n depends on (χ) because of the effect of global circulation and chemistry) [9]. As

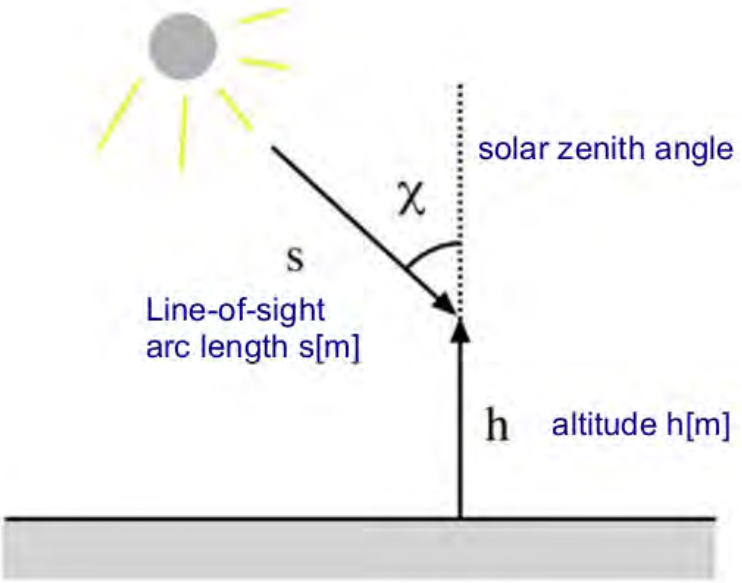

Figure 1.2: illustration showing the line-of-sight path length S, the solar zenith angle χ and the altitude h

the radiation is absorbed, its intensity decrease as

$$-\frac{dI}{ds} = \sigma n_n I \tag{1.9}$$

where I is intensity of radiation (energy flux, electron volts per square meter per second);
s is line-of-sight path length;
n_n is density of neutrals (per cubic meter);
σ is photon-obsorption cross section (square meter);
Because the rate of ion production should be proportional to the rate at which radiation is absorbed, we can write

$$Q = -C\frac{dI}{ds} = C\sigma n_n I \tag{1.10}$$

where C is the number of electrons produced in the absorber per unit energy absorbed and it is constant. The production rate Q reaches a peak (along s) when

$$C\sigma(I\frac{dn_n}{ds} + n_n\frac{dI}{ds}) = 0 \tag{1.11}$$

Or

$$\frac{dQ}{ds} = 0 \tag{1.12}$$

But s is related to h by ds = -dhsec χ (fig.1.2), and because

$$\frac{1}{n_n}\frac{dn_n}{ds} = -\frac{1}{n_n}\frac{dn_n}{dh}\cos\chi = \frac{\cos\chi}{H_n} \tag{1.13}$$

for the peak or maximum of production, the equation gives

$$\sigma H_n n_{max} \sec\chi = 1 \tag{1.14}$$

Or

$$\sigma N_{nmax} = 1 \tag{1.15}$$

Where N_{nmax} is the integrated density N_{nmax} = $\int_{\infty}^{s_{max}} n_n ds$ along the line of sight up to the postion of the peaks s_{max}.
From equation (1.9)

$$\frac{dI}{I} = d\ln I = -\sigma n_n ds \tag{1.16}$$

Integrating

$$\int_{\infty}^{s} d\ln I = -\int_{\infty}^{s} -\sigma n_n ds = -\sigma N_{ns} \tag{1.17}$$

$$\ln(\frac{I(s)}{I(\infty)}) = -\sigma\int_{\infty}^{s} n_n ds = -\sigma N_{ns} \tag{1.18}$$

Or

$$I(s) = I(\infty)\exp(-\sigma N_{ns}) \tag{1.19}$$

$$= I(\infty)\exp(-\tau) \tag{1.20}$$

where τ is the optical depth. At the peak, σN_{ns} = σN_{nmax}=1, so the peak is the altitude where the optical depth is unity. Both the radiation intensity at the top of the atmosphere of the atmosphere and σ vary for different wave lengths.
Then the producrion rate is

$$Q_{max}(\chi,h) = C\sigma n_{max} I_{max} = C\sigma(\sigma H_n \sec\chi)^{-1}(I(\infty)\exp(-1)) = \frac{CI(\infty\cos\chi)}{H_n\exp(1)} \tag{1.21}$$

By using the neutral-gas altitude profile n_n = $n_o\exp(\frac{-h-h_o}{H_n})$, we can determine the height of the production peak h_{max} by writing:

$$\sigma H_n n_{max}\sec\chi = 1 = \sigma H_n n_o \exp(-\frac{h_{max}-h_o}{H_n})\sec\chi \tag{1.22}$$

Similarily by solving for h_{max}, we can determine the dependence of the radiation intensity I on h by using the earlier experssion for I(s) and noting the N_{ns} is the integrated density along the line of sight;

$$I(h) = I(\infty)\exp[-\sigma n_o H_n \sec\chi\exp(-\frac{h-h_0}{H_n})] \tag{1.23}$$

The dependence of the production rate Q on h and χ is given by

$$Q(\chi, h) = C\sigma n_n I = C\sigma n_o I(\infty) \exp[-\frac{h - h_o}{H_n} - \exp(-\frac{h - h_o}{H_n})] \tag{1.24}$$

With $CI(\infty) = \frac{Q_{max} \exp(1) H}{\cos \chi}$, finally the rate production is given by

$$Q(\chi, h) = Q_{max} \exp[1 + \frac{h_{max} - h}{H_n} - \exp(\frac{h_{max} - h}{H_n})] \tag{1.25}$$

But $y = \frac{h - h_{max}}{H_n}$ implies

$$Q(\chi, h) = Q_{max} \exp[1 - y - \exp(-y)] \tag{1.26}$$

$$Q(\chi, h) = Q_{max} \exp[1 - \frac{h - h_{max}}{H_n} - \exp(-\frac{h - h_{max}}{H_n})] \tag{1.27}$$

which is the chapman production function. The rate Q is the rate of production of both ions and photoelectrons, because these usually are produced in pairs.

1.4 Ion Loss

Ionosphere is so cold that it needs a continuous ionization (day-night asymmetry). Ionospheric electrons disappear by virtue of three types of recombinations such as Radiative recombination, Dissociative recombination and Attachment
Radiative recombination is given by

$$e + x^+ \longrightarrow x + h\nu \tag{1.28}$$

while dissociative recombination

$$e + xy^+ \longrightarrow x + y \tag{1.29}$$

and attachment

$$e + z \longrightarrow z^- \tag{1.30}$$

The most important dissociative recombination processes in the atmosphere are:

$$O_2^+ + e \longrightarrow O + O \tag{1.31}$$

$$N_2^+ + e \longrightarrow N + N \tag{1.32}$$

The first two recombinations of these are most important through out the bulk of the ionosphere. i.e Radiative recombination is responsible for many types of observed airglows. In contrast, most of the emission that one sees in an aurora occurs when atomic and molecular elecrons are excited to higher energy level by coulomb collision with the passing precipitating particles and then undergo radiative de-excitation. Recombination occurs at rates that depend on the local concentration of the ions and electrons;

$$L = \alpha n_e n_i \tag{1.33}$$

where n_e are the electron and ion densities and α is a recobination coefficient. The recombination ion coefficient is determined by emperical and theoretical method [5].

1.5 Transport process in the ionosphere

The first order correction is the vertical transport, because the ionosphere is a thin layer where altitude variability is much larger than horizontal variability. We can restrict our attention to the vertical transport attributable to the vertical velocity u_n. The equlibrium electron density distribution must then satisfy the vertical-continuity equation [9]:

$$\frac{\partial n_e}{\partial t} = Q - L - \frac{\partial n_e u_{eh}}{\partial h} \tag{1.34}$$

where the new influnce on the electron density is the vertical-flux gradient, which describes the difference between the flux of electron entering and leaving a given altitude. In order to find the velocity u_{eh}, we need to invoke other equation. The momentum or force balance equation:

$$-\frac{dp_e}{dh} - n_e m_e g - e n_e [E_h + (u_e \times B)_h] = n_e m_e \nu_{eh}(u_{eh} - u_{nh}) + n_e m_e \nu_{ei}(u_{eh} - u_{ih}) \tag{1.35}$$

$$-\frac{dp_i}{dh} - n_e m_i g + q n_e [E_h + (u_i \times B)_h] = n_e m_i \nu_{in}(u_{ih} - u_{nh}) + n_e m_i \nu_{ei}(u_{ih} - u_{eh}) \tag{1.36}$$

where
p_e = electron thermal pressure $n_e \mathrm{k} T_e$;
p_i = ion pressure $n_e \mathrm{k} T_i$;
g = gravitational acceleration;
E = eletric field;
B = magnetic field;
u_e = electron velocity;
u_i = ion velocity;
ν_{en} = electron-neutral collision frequency;
ν_{in} = ion-neutral collision frequency;
ν_{ei} = electron-ion(coulomb) collision frequency; and
u_n = neutral velocity.
By adding equation (1.35) and equation (1.36) and assumed that ions are singly charged (q = e) that the ions and electrons vertical drift togther at velocity u_{pl} (to maintain charge neutrality in the plasma). Then we obtain

$$u_{pl} - u_{nh} = -\frac{1}{n_e m_i \nu_{in}} [\frac{d}{dh}(p_i + p_e) + n_e m_i g] \tag{1.37}$$

Furthermore, if the tempratures are all assumed to be independent of h, and the vertical velocity u_{nh} is zero. The forgoing equation can be written in the form of a diffusion equation for n_e:

$$u_e u_{pl} = -D[\frac{dn_e}{dh} + \frac{n_e}{H_p}] \tag{1.38}$$

where D = $\frac{k(T_i+T_e)}{m_i \nu_{in}}$ is called ambipolar diffusion coefficient, and H_p is the "plasma scale height"

$$H_p = \frac{k(T_i + T_e)}{m_i g} \tag{1.39}$$

In general, u_i and u_e have horizontal as well as vertical compnents. For special case where B is horizontal Ampere′s low for the current density j:

$$j = n_e e(u_i - u_e) = \frac{\bigtriangledown \times B}{\mu_o} \tag{1.40}$$

By using equation (1.40), the vertical transport velocity becoms

$$u_{pl} = -\frac{1}{n_e m_i \nu_{in}}[\frac{dp_T}{dh} + n_e m_i g] \tag{1.41}$$

where p_T = total pressure(thermal plus magnetic) = $n_e(T_i+T_e) + \frac{B^2}{2\mu_o}$

1.6 Ionospheric Variations

The ionosphere varies in systematic ways because the main source of ionization solar UV and X-rays intensity depend on the position of the sun in the sky at a particular location on Earth and on the sun′s absolute output. When the sun is directly over head, the intensity of sunlight reaching the upper atmosphere is greatest. As the observer either moves towards the poles or to the day-night terminator, the intensity decrease because the angle sun make with the upper atmosphere is more oblique. As the observer moves into the dark or night side hemisphere of Earth, the amount of sunlight goes to zero and production due to photoionization ceases. The rotation and curvature of Earth therefore give rise to variation in the ionospheric structure [8].

Daily Variations

The day-night variation is due to Earth′s rotation. Night time electron densities are much lower than day time values, because of higher recombination rates in the absence of radiation source. Day time electron densities typically reach their peak at hours past local noon due to the Earth′s atmosphere lagging two hours behind the solid Earth′s rotation [6].

Seasonal Variations

At different time of year the sun is vertically above different geographic locations. At equinox noon (March 21, September 23) the sun is vertically above observer at the equator and vertically above observer at the Tropics of Capricon and Cancer or solstice dates (21 December and 21 June). As vertical illumination from the sun results in higher ionization rates, higher electron density concentration are observed at these locations on these dates than at other locations [6].

Latitudinal Variations

Similar to diurnal and seasonal variation, The sun′s position relative to the atmosphere plays a significant role in latitudinal variation of ionospheric densities. The solar zenith angle, χ the angle measured from an observer′s local vertical to the sun, determine the intensity of ionization where locations with small zenith angle are exposed to higher radiation rates. The sun′s zenith angle at Tropic of Capricon (23.5^0 s) at noon on 21 March (southeren Autum equinox) will be 47^0, with expected lower ionization rates and densities than at the Tropic of cancer where the sum will be vertically over head (zenith angle of 0^0) [6].

Solar Cycle Variations

Solar cycle variations refer to the ionosphere′s response to increased sunspot activity or sporadic phenomena like coronal mass ejections, solar flares or x-ray flares, all of which

introduce raised level of radiation, resulting in increased plasma densities in the ionosphere [6]. The solar activity variation is linked to the 11-years solar cycle. During the period of maximum sunspot number, which occur when the solar cycle is at its peak, the ionization is greater than at solar minimum because the solar radiation intensity is high thus enhancing the electron concentration in the ionsphere. The solar disturbance are more frequent at solar maximum than solar minimum [5].

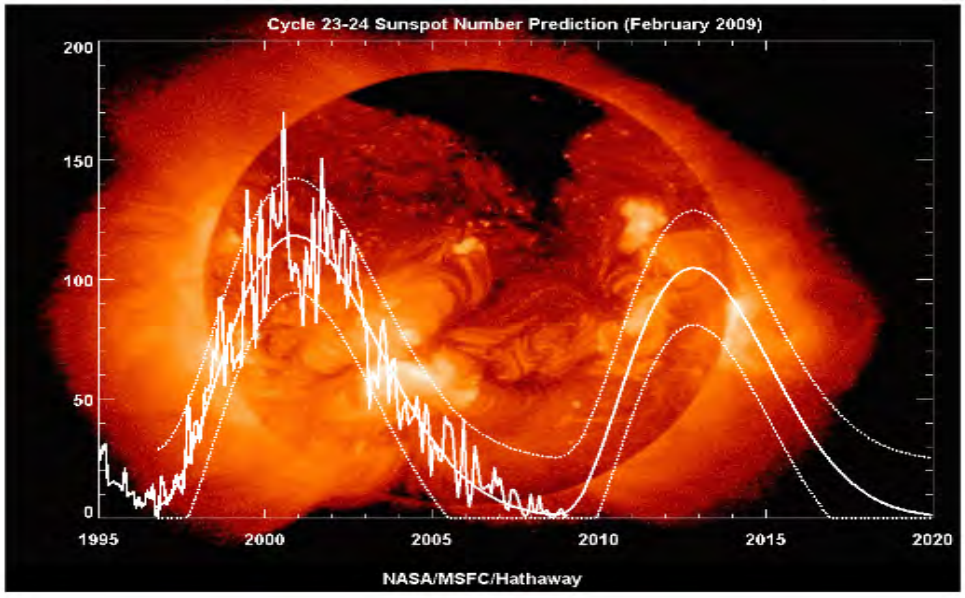

Figure 1.3: Solar cycle(source: http://solar-center.stanford.edu).

1.7 Major Geographic Regions of the Ionosphere

There are three major regions of the global ionosphere. These are the high-latitude, mid-latitude and equatorial regions [3]. Ethiopia is found in Equatorial magnetic region with the magnetic equator passing through Addis Ababa

Equatorial Region

At the equator, the magnetic field is nearly horizontal to the surface of the earth. Because of his special geometry, there is an intense current sheet, known as the equatorial electrojet, which flows along the magnetic equator at about 110 km altitude (E region) in a strip a few degrees wide in latitude. The current flows toward the east in the day where the ionospheric density is high in the E region. There is a west ward flow at night, but this is nearly undetectable because of the small electron concentrations at night time.
The eletric field associated with these ionosperic current drive a plasma convection in the F region at low latitude that is upward and westward in day time. This up ward motion takes freshly ionized plasma to higher altitudes where it recombines very slowely. This plasma which has moved up, now flows under the influence of gravity down the magnetic field lines to higher latitude ($+20^0$ or -20^0) both North and South and results in regions of increased electron concentration in two bands parallel to the geomagnetic equator. This phenomenon give rise to the so-called " Equatorial or Appleton" (lower electron density at the equator and

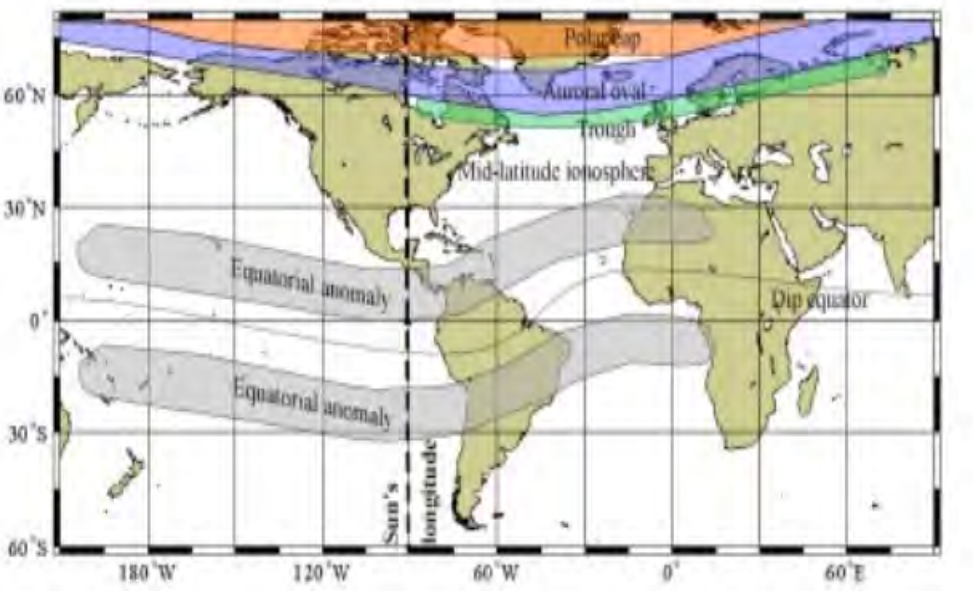

Figure 1.4: Major geographic regions of the ionosphere (after Bishop et al. [1991]).

higher electron density at $+20^0$ or -20^0). As a result of these and other physical processes, day time critical frequencies for all equatorial ionospheric layer are generally higher than at midlatitudes. There is little particle precipitation at low latitudes so that in this region ionization is produced primarily by solar EUV radiation [10].

Mid-Latitude Region

The mid-latitude ionosphere is the least variable and undisturbed among the different ionospheric regions. It is usually free of the effect imposed by the horizontal magnetic field geometry peculiar to the equatorial region. Also, this is the region from where we have most of the ionospheric observations available due to the fact that most of the ionosphere-sensing instruments are located in countries situated in the mid-latitude region [3].

High-Latitude Region

The high latitude ionosphere is a product not only of the solar radiation and the terrestrial effect, but also solar-magnetospheric effect. These result from the interaction of the magnetic field of the earth with the solar wind, the plasma (chiefly ionized hydrogen and electrons) boild off from the sun. There are two general phonomena of magnetosphere origin, the aurora and ionospheric - magnetospheric convection. Together they produce a multitude of varying and overlapping effect that are permanent features of the high latitude ionosphere. These large effects often produce rapidly varying level of electron density [10].

1.8 Ionospheric Disturbances

Ionospheric disturbances can result from solar disturbances or geomagnetic field disturbances. The ionospheric disturbances are associated directly or indirectly with the events on the sun. The geomagnetic disturbances are also caused by events initiated from the sun, however,

these events rather affect the outermost geomagnetic field line (also called the magnetopause) and compress the geomagnetic field causing the geomagnetic disturbances [3].

1.9 Ionospheric Storms

Ionospheric storms can be caused by intense solar eruptions hurling out energetic particles also known as solar flares that can endanger astronauts and destroy satellite electronics [3]. During a global ionospheric storm electron density can decrease to some minimum value and then slowely recover. Succesive storm may cause additional reduction in electron density, but some absolute minimum value exist at any point. The storm can not turn off electron production, since that depend primarily on sunlight. During the recovery phase, which may last a day or less at solar maximum to a month at solar minimum, day time increase will initially over balance night time loss as the ionospheric refills. After a weak, diurnal variation will be comparable to quite monthly extremes. Similar conditions occur in conjuction with auroral substorms except that the resulting density depletions are typically continued to the summer day light sector located near middle geomagnetic latitudes. The dipressions then corotate with the Earth until they dissipate. Magnetospheric electrons, precipitating with the aurora zone, collide with and ionize neutral atmospheric molecules. This releases secondary electron which enhance auroral E-region densities until storm condit-ions subside [11]. In general, when the electron densities increase as a result of storm dynamics, it is called a positive ionospheric storm, whereas a decrease in electron density is called a negative ionospheric storm [12].

1.10 Geomagnetic Storms

Geomagnetic storms usually occur in conjunction with ionospheric storms and can be caused by solar flares, high speed solar wind stream (coronal holes) and sudden disappearing filaments. The storms are usually associated with increased electron densities in the lower ionosphere and a simultaneous increase in absorption of radio waves. A geomagnetic storm usually starts with an increase in the earth's geomagnetic field intensity called the initial phase followed by a large decrease termed the main phase. A solar-flare originated geomagnetic storm usually starts with a sudden commencement as an initial phase. On the other hand, a high speed solar wind stream induced geomagnetic storm is expected to start with a gradual commencement with storms tending to reoccur every 27 days or so following the sun's rotation [3].
A geomagnetic storm has three distinct phase: the initial phase, the main phase and the recovery phase. The initial phase characterised by an increase in the magnetic field, which is caused by the compression of the magnetosphere when the increased solar wind arrives, and lasts for a few hours. The main phase is characterised by a sustained south-ward interplanetary field and can last several hours. The main phase is followed by a slow return to normal conditions that is recovery phase which can last over a few days [5].

1.11 Ionospheric Scintillation

There are certain regions of the ionosphere (mainly the high and low latitude F-region) and the ionosphere may become highly turbulent. "Turbulence" is defined here as presence of

small-scale (from centimeters to meters) structure or irregularities imbedded in the large-scale (tens of killometers) ambient ionosphere. Under favorable conditions, plasma density irregularities are generated just after sunset in the equatorial region and may last for several hours. At high latitudes, these irregularities may be genrated during either the day time or at night time. For both low and high latitude regions these small-scale irregularities occur most frequently during the solar cycle maximum period. The existence of these small-scale structures can seriously affect the nature of radio waves as they propagate through the ionosphere where they are imbedded. Radio wave propagating through a "clear" environment that aburptly become filled with small-scale irregularities. The term "ionosphere scintillation" has been used to describe this effect on the radio signals. The bigger the amplitude fluctuations of the scintillated signal the greater the impact on communication and navigation systems [13].

1.12 Ionosphere Models

International Reference Ionosphere (IRI)

The IRI is an international project sponsored by the Committee on Space Research (COSPAR) and the International Union for Radio Science (URSI). For a given geographic location, time and date,the IRI model describes the elecron density, electron temperature, ion temperature and ion composition (O^+, H^+, He^+, NO^+, O_2^+), ion drift and Total Electron Content (TEC) in the altitude range 50 up to 2000 km. IRI provides monthly averages in the non-auroral ionosphere for magnetically quiet conditions. The major data sources for the IRI model development are the world-wide network of ionosondes, incoherent scatter radar, satellite top side sounders and in situ instruments on several satellites and rockets [3].

Bent Ionospheric Model

The model describes the ionospheric electron density as a function of latitude, longitude, time, season, and solar radio flux. The topside is represented by a parabola and three exponential profile segments, and the bottomside by a bi-parabola. The model is based on about 50,000 Alouette topside ionograms (1962-1966), 6,000 Ariel 3 in situ measurements (1967- 1968), and 400,000 bottomside ionograms (1962-1969). For the F2-peak the CCIR maps are used. The model has been widely used for ionospheric refraction corrections in satellite tracking. It does not include the lower layers (D, E, F1) and uses a simple quadratic relationship between CCIR's M(3000)F2 factor and the height of the F2-peak. A comparison between the Bent model and the IRI model and their application for satellite orbit determination was discussed by Bilitza. IRI showed better results because of the more detailed representation of the bottomside density structure [14].

PIM Model

The Parameterized Ionospheric Model (PIM) is a climatology model built from combining model output from the Global Theoretical Ionospheric Model (GTIM) model for low and middle latitude with output from the TDIM model for high latitudes and from the empirical model for plasmaspheric altitudes. The altitude profiles obtained with these models was then represented by empirical orthonormal functions (EOF). The resulting set of several million coefficients constitutes the PIM model. EOFs have the advantage of a simple and

straightforward fitting process different from the non-linear schemes required for Chapman functions. But EOFs do not include the peak density and height as explicit parameters. To get these parameters the full profile has to be constructed and then a peak-finding algorithm has to be applied. PIM consists of portable FORTRAN source code and a large database of coefficients for the orthogonal function expansion. For user specified geophysical conditions and spatial coordinates, PIM produces electron density profiles (EDPs) between 90 and 25000 km altitude, corresponding critical frequencies and heights for the ionospheric E and F2 regions, and Total Electron Content (TEC).
The Parameterized Real-Time Ionospheric Specification Model (PRISM) is a version of PIM with data assimilation capabilities. The GTIM evolved from a low-latitude, to a mid-latitude and finally global model. It computes O^+, H^+ and He^+ densities along magnetic field lines from 90 to 1600 km. In addition to the standard empirical input models for thermospheric parameters, solar EUV, ExB drift pattern, and precipitating energetic electrons, GTIM also requires the ion and electron temperatures as input parameters. To provide an easy accessible version of the GTIM model, output parameters were computed on a global grid and then fitted with Chapman functions. The set of Chapman parameters constitutes the Semi-Empirical Low Latitude Ionospheric Model (SLIM). An analytical version of the SLIM model, the Fully-Analytical Ionospheric Model (FAIM), was produced on the basis of the Chiu model formalism by altering the low latitude portion of this model so that it reproduces the SLIM profiles. The GTIM, SLIM, FAIM, PIM and PRISM family of models was developed at the US Air Force Research Laboratories [15].

NeQuick model

NeQuick model is a quick-run ionospheric electron density model particularly designed for trans-ionospheric propagation applications. To describe the electron density of the ionosphere up to the peak of the F2 layer, the NeQuick uses a profile formulation which includes five semi-Epstein layers with modelled thickness parameters. Three profile anchor points are used: the E layer peak, the F_1 peak and the F_2 peak, that are modelled in terms of the ionosonde parameters foE, foF1, foF2 and M(3000)F_2. These values can be modelled (e.g. ITU- R coefficients for foF_2, M3000) or experimentally derived. A semi-Epstein layer represents the model topside with a height- dependent thickness parameter empirically determined. The NeQuick gives the electron density for positions in the ionosphere with height, geocentric latitude, geocentric longitude as coordinates on a spherical earth. The model values depend on solar activity (given by monthly-mean sunspot number R12 or 10.7 cm solar radio flux F10.7) season (month) and time (Universal Time UT) [16].

1.13 Importance of the Ionosphere

At great height, the air is thin: only about one millionth of all atmospheric particle is located above 100 km altitude. Of these, only a small fraction is ionized. Still, the ionsphere is some of importance to mankind. The first and the foremost result of the presence of the ionosphere, or rather the upper atmosphere, is the protection of life on earth from the dangerous ionizing radiation from the sun and the rest of the universe. The radiation is obsorbed by the process of photoionization. This pertains to the high energy end of the solar spectrum, from roughly hydrogen's Lyman-α line, at wave length of λ=122nm, to shorter wave length. Outside the earth's atmosphere, the flux in this part of the solar spectrum is about 8mWm^{-2}, on a total bolometric flux of 1.4kWm^{-2}. The high energy ends of the solar spectrum strongly varies

and the more so in periods of high solar activity. It is intersting to compare the ionosphere's protective working to that of the stratospheric ozon layer. O_2 and especially O_3 abosrb solar radiation in the range from Lyman-α to $\lambda \approx 300$nm, by the process of photodissociation. One might therefore state that the ionosphere is equally important to life on earth as the ozone layer. This is only partially true, however, because the total power absorbed in the ozone layer is a few hundred times larger the power obsorbed in the ionosphere. More reassuring in this respect the fact that we will never see the apperance of a hole in the ionosphere, because the outer most part of the atmosphere is always ionized. Therefore, the ionosphere can only disappear when the whole atmospehre vanishes. Although of vital importance, it is obvious that the protective aspect of the ionosphere does not generate much enthusiasm for research [17].

Chapter 2

Cosmic Data and Radio Occultation Technique

2.1 Introduction

Data from the Constellation Observing System for Meteorology and Climate (COSMIC) has provided a new and revealing light on a wide variety of natural phenomena that are of considerable importance to the scientific communtiy and to a society as a whole. COSMIC is an interdisplinary satellite mission that address some of the most in triguing question in the Earth science today. In the ionosphere COSMIC data accelerate the development of physical model for space weather predication by providing dense, accurate, and global electron density measurements for model testing The large volume of high quality ionospheric observations from COSMIC significantly advance space weather research. Scientists are able to observe the response of the global ionosphere to the impact of a solar storm as its effects propagation around the globe. New revelations from this data set has improve physicale ionospheric models and thus contribute to the development of predictive skills for space weather [18].
The FORMOSAT-3/COSMIC satellite were lounched successfully on April 15, 2006 and their orbits at about 800 km height. The inclination angle and period of each satellite are 72^0 and about 100 minutes, respectively. There are three payloads on board each COSMIC satellite, namely, 4 sets of GPS signal recivers, a Tri-band (150, 400, and 1067 MHz) becon transmitter system, and a tiny ionospheric photometer at 135.6 nm, for weather/climate, ionosphere and geodesy research and applications. The six COSMIC satellites in their orbit can provide 2,500 vertical soundings of the ionospheric electron density per day. Presently, there are around 1800 neutral atmospheric profiles per day available due to different reasons [19]. Radio occultation (RO) methods are also being increasingly investigated . RO measurements are made by monitoring transmissions from GPS satellites using receivers on low earth orbiting (LEO) satellites and provide the potential of measuring refractivity profiles in regions where ground based sensors cannot easily be located, such as deep sea waters [20].
In the following sections, we describe different aspects of cosmic instrument and data retrieval. The COSMIC STEC is used to compliment STEC from ground-based GPS recievers. However, we do not give detail STEC determination from ground-based GPS recievers since complete description is given in a thesis work of Kidanu [21].

2.2 Principl of Radio Occultation Technique

In order to make accurate radio occultation inversions, the clock drifts of the GPS transmitter and reciever clocks should be removed from the raw phase data in order to solve the bending angles derived from the Doppler L_1 phase excess. Other wise, a completely unrealstic result (several orders of magnitude higher) would be obtaind. The basic observable is the phase

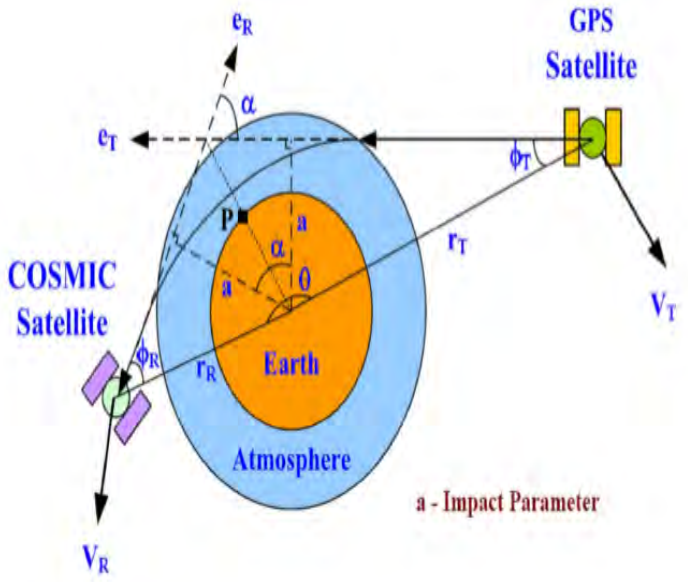

Figure 2.1: COSMIC and GPS satellite ray path (from Chu, Y.H lecture, 2007)

path (expressed in meters)

$$L = \int_{GPS}^{LEO} nds \tag{2.1}$$

where L stands for either L_1 or L_2 carrier phase observables, n refraction index and the integral extends from the LEO postion up to GPS one. From the phase path, the excess phase is defined as

$$\Delta L = L - |\vec{r}_{LEO} - \vec{r}_{GPS}| \tag{2.2}$$

The observable needed is the phase change, the so-called excess Doppler or Doppler shift

$$f_d = \frac{d\Delta L}{dt} \tag{2.3}$$

The Doppler shift at both the transmitter and the reciever is produced by the atmospheric and ionospheric refraction index change, after subtracting the velocity of both transimiter and reciver projected along the actual propagation direction. The signal Doppler shfit f_d becomes the fundamental observable. The Doppler shift of the oprating frequency f_T can be drived using

$$f_d = -\frac{f_T}{c}(\vec{V_T} \bullet \vec{e_T} + \vec{V_R} \bullet \vec{e_r}) = -\frac{f_T}{c}(V_T^r cos\phi_T + V_T^\theta sin\phi_T + V_R^r cos\phi_R - V_R^\theta sin\phi_R) \tag{2.4}$$

where V_T^r and V_T^θ represent the radial and tangent components of the transmitting spacecraft velocity.
Under spherical symmtery, the senll′s law becomes Bouguer′s rule,

$$nrsin\phi = a = constant \tag{2.5}$$

and $a = nr_t$, where r_t is the radius at the tangent point along the ray path.
From the geometry in Fig. 2.1 we have :

$$r_T sin\phi_T = r_R sin\phi_R = a \tag{2.6}$$

$$2\pi = \phi_T + \phi_R + \theta - \pi \tag{2.7}$$

so that

$$\alpha = \phi_T + \phi_R + \theta - \pi \tag{2.8}$$

with θ is the angle between the transmitter and reciver position vectors.

2.2.1 The way to estimate bending angle α

The Doppler equation for the straight line path is

$$f_{d0} = -\frac{f_T}{c}(V_T^r cos\phi_{T0} + V_T^\theta sin\phi_{T0} + V_T^r cos\phi_{R0} - V_T^\theta sin\phi_{R0}) \tag{2.9}$$

Using Taylor expression, we have the following relations

$$\begin{aligned} sin(\phi_T) &= sin(\Delta\phi_T + \phi_{T0}) \cong sin(\phi_{T0}) + cos(\phi_{T0})\Delta\phi_T \\ cos(\phi_T) &= cos(\Delta\phi_T + \phi_{T0}) \cong cos(\phi_{T0}) - sin(\phi_{T0})\Delta\phi_T \end{aligned} \tag{2.10}$$

where $\Delta\phi_T = \phi_T - \phi_{T0}$ The difference between Doppler frequencies and straight paths is the atmospheric Doppler contribution, f_{atm}, which is given as

$$f_{atm} = f_d - f_{do} = \frac{f_T}{c}(V_T^r sin\phi_{T0} - V_T^\theta cos\phi_{T0})\Delta\phi_T + (V_T^r sin\phi_{R0} + V_T^\theta cos\phi_{R0})\triangle\phi_R \tag{2.11}$$

Notice that V_T^r and V_T^θ are perpendicular to the straight line path. So the relevant velocity

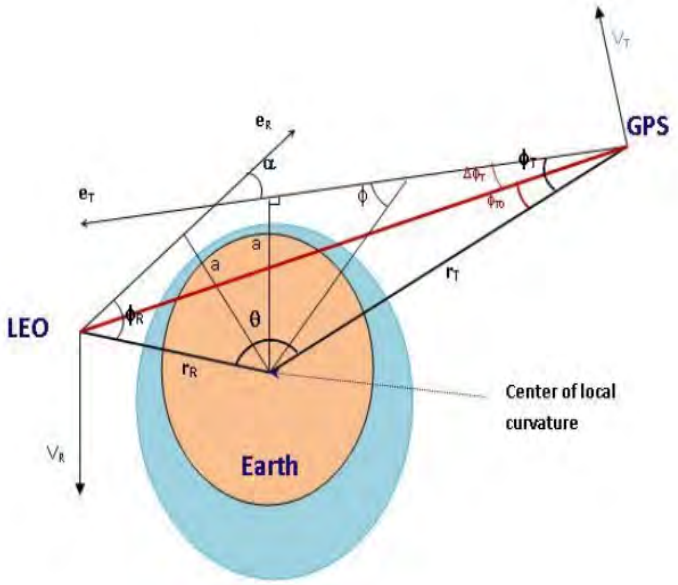

Figure 2.2: Bending angle α in RO technique (from Dao Ngoc Hanh Tam, Graduate paper)

responsible for the atmospheric Doppler shift is the descent or ascent velocity of the straight

line path.
From the Taylor expansion of Bouguer′s rule, we have

$$r_T cos(\phi_{T0})\Delta\phi_T = r_R cos(\phi_{R0})\Delta\phi_R \tag{2.12}$$

So that

$$\frac{\Delta\phi_R}{\Delta\phi_T} = \frac{r_T cos(\phi_{T0})}{r_R cos(\phi_{R0})} \tag{2.13}$$

For the GPS-LEO occultaton geometry, we have

$$\frac{\Delta\phi_R}{\Delta\phi_T} = \frac{r_T cos(\phi_{T0})}{r_R cos(\phi_{R0})} \sim 9 \tag{2.14}$$

From Fig. 2.2, we know that

$$\Delta\phi_T + \Delta\phi_R = \alpha \tag{2.15}$$

so,

$$\alpha = 1.1\Delta\phi_R \sim \Delta\phi_R \tag{2.16}$$

Consequently, we can write the atmospheric Doppler contribution, f_{atm}, as

$$f_{atm} \cong \frac{f_T}{c} V_\perp \alpha \tag{2.17}$$

where f_{atm} can be measured from the observed Doppler frequency of LEO satellite and α can thus is estimated.
So the atmospheric Doppler is linearly proportional to bending angle, and the straight line Descent velocity is typically 2 to 3 km/sec. Therefore, by using Taylor expression above and Bouguer′s rule, the impact parameter a can be approximated as

$$a \sim r_R sin(\phi_{R0}) + r_R cos(\phi_{R0})\alpha \tag{2.18}$$

or

$$a \cong r_R sin(\phi_{R0}) + r_R cos(\phi_{R0}) \frac{c f_{atm}}{f_T V_\perp} \tag{2.19}$$

2.2.2 Relation between bending angle and refractivity gradient

The differentail equation for ray path can be derived as

$$\frac{d}{ds}(n\frac{d\vec{r}}{ds}) = \nabla n \tag{2.20}$$

where $\vec{r}$ is position along the ray path and ds is an incremental length along the ray path such that

$$d\vec{r} = \hat{s}ds \tag{2.21}$$

where $\hat{s}$ is the unit vector in the direction along the ray path
Consider the change in the quantity, $\vec{r} \times n\hat{s}$, along the ray path is given as

$$\frac{d}{ds}(\vec{r} \times n\hat{s}) = \frac{d\vec{r}}{ds} \times n\hat{s} + \vec{r} \times \frac{d}{ds}(n\hat{s}) = \vec{r} \times \frac{d}{ds}(n\hat{s}) \tag{2.22}$$

This equation shows that only the non-radial portion of the gradient of index of refraction contributes to changes in $\vec{r} \times n\hat{s}$
So, for spherical symmetric atmosphere

$$a = nrsin\phi = constant \qquad (Bouguer's \quad rule) \tag{2.23}$$

This signal path is curved according to Snell′s law because of changes in the index of refraction along the path. To first approximation, we assume the refractivity changes only as function of radius.
From Bouguer′s rule above, we have

$$d(nrsin\phi) = 0 = rsin\phi dn + nsin\phi dr + nrcos\phi d\phi \tag{2.24}$$

$$d\phi = -\frac{dr(rsin\phi\frac{dn}{dr} + nsin\phi)}{nrcos\phi} \tag{2.25}$$

Notice that the equation for a straight line in polar coordinate is

$$rsin\phi_o = const \tag{2.26}$$

So, for the straight line

$$d\phi = -\frac{drsin\phi_o}{(rcos\phi_o)} \qquad (i.e\frac{dn}{dr} = 0 \quad and \quad n = 1) \tag{2.27}$$

So the change in direction of the path or the bending along the path (with curving downward defined as positve) is

$$d\alpha = d\phi_o - d\phi = \frac{dr(rsin\phi\frac{dn}{dr})}{nrcos\phi} = \frac{dr\frac{a}{n}\frac{dn}{dr}}{nr[1 - sin^2\phi]^{\frac{1}{2}}} \tag{2.28}$$

Therefore

$$d\alpha = dr\frac{dn}{ndr}\frac{a}{\sqrt{n^2r^2 - a^2}} \tag{2.29}$$

The total bending is the integral of $d\alpha$ along the path

$$\alpha = \int d\alpha = 2\alpha\int_{r_t}^{\infty} dr\frac{dn}{ndr}\frac{1}{\sqrt{n^2r^2 - a^2}} \tag{2.30}$$

We measure profiles of $\alpha(a)$ from Doppler shift. The term that we want to know is profiles of n(r)
Via an Abel integral transform referring to special class of integral equations deduced by Abel by 1825 which are a class of Volterra integral equations (Tricomi, 1985)
Firstly, we rewrite in terms of x=nr rather than r:

$$\alpha(a) = 2a\int_{x=a}^{x=\infty} \frac{dn}{ndx}\frac{dx}{\sqrt{x^2 - a^2}} \tag{2.31}$$

Multiplying each side of above equation by the Kernel, $\sqrt{a^2 - a_1^2}$, and integrating a from a1 to infinity

$$\begin{aligned}\int_{a1}^{\infty} \frac{\alpha(a)da}{\sqrt{a^2 - a_1^2}} &= \int_{a=a1}^{a=\infty} \frac{2a}{\sqrt{a^2 - a_1^2}}[\int_{a=a1}^{a=\infty} \frac{dn}{ndx}\frac{dx}{\sqrt{x^2 - a^2}}]da \\ &= \int_{x=a1}^{x=\infty} \frac{dn}{ndx}[\int_{a=a1}^{a=x} \frac{2ada}{\sqrt{a^2 - a_1^2}\sqrt{x^2 - a^2}}]dx \\ &= \int_{x=a1}^{x=\infty} 2\frac{dn}{ndx}[sin^{-1}\sqrt{\frac{a^2 - a_1^2}{x^2 - a_1^2}}]_{a=a1}^{a=x}dx \\ &= \pi \int_{x=a1}^{x=\infty} \frac{dn}{ndx}dx = -\pi ln[n(r_{01})]\end{aligned} \tag{2.32}$$

Therefore

$$n(r_{01}) = \exp[-\frac{1}{\pi}\int_{a1}^{\infty} \frac{\alpha(a)da}{\sqrt{a^2 - a_1^2}}] \tag{2.33}$$

Note that $r_{01} = a_1/n(a_1)$
The atmospheric refractive index is defined as

$$n = 1 + (77.6\frac{p}{T} + 373000\frac{p_w}{T^2}) \times 10^{-6} - 40.3\frac{N_e}{f^2} \tag{2.34}$$

where p = atmospheric pressure;
p_w = water vapor pressure;
T = temprature (in Kenvin);
N_e = ionospheric electron density ($electrons/m^3$); and
f = radio wave frequency (Hz).
In the ionosphere, altitude higher than 90 km, the contributions of temprature, pressure and water vapor pressure t atmospheric refractive index are negligible compared to free electron density contribution. Furthermore, in light of the fact that L_1(=1.57542 GHz) and L_2(= 1.22760 GHz) frequencies of the GPS signals are much greater than electron gyro-frequency (about 1 MHz) and electron-neutral collision frequency (about 1 KHz in F region), the relation between atmospheric refractive index n and ionospheric electron density N_e can be approximated to

$$N_e = \frac{(1 - n)f^2}{40.3} \tag{2.35}$$

where f is GPS frequency in unit Hz and N_e is the electron density in unit $electrons/m^3$. As a result, N_e can thus be obtained from occultation-measured in accordance with this equation.

2.3 Algorithms for Radio Occultation Inversions in the Ionosphere

For COSMIC, the inversion method for ionosphere radio occultation is based on an assumption of local spherical symmetry. The assumption is that the electron density within a few thousand kilometers radius around the tangent point of the ray path is locally spherically symmetric. This assumption cannot always be valid since it ignores the physical presence of

horizontal density gradients. The retrieved electron density profile may have errors in cases when ionospheric conditions differ greatly from assumptions. In particular, for altitudes below the E region negative values can often be found in the density profiles generated by CDAAC. Another issue of note is that the vertical electron density profile is determined for different horizontal geographic locations of the ray path bottom versus top; the horizontal distance bottom versus top of the profile can be one hundred kilometers. The profile does not represent the ionosphere for the same longitude and latitude at different altitudes.
Phase measurements of the RO signal are fundamental observations necessary to derive the refractivity. The refractivity is then used to derive the electron density profile in the ionosphere (or temperature and pressure profile in the neutral atmosphere). Abel inversion is a common technique for processing RO data which is sensitive to vertical structures. The GPS/MET mission was the first to perform the application of Abel inversion to RO retrieval. Usually there are two types of retrieval based on different kinds of observations. One is based on bending angle. The other is based on slant total electron content (STEC) observations [22].

2.3.1 Abel Inversion

In physics or engineering it is common to have two functions such that one is the integration of the other: $f(a) = \int_a^b g(t)k(\omega, t)dt$. The function f(a) is the integral transform of the function g(t). As the integral transforms comprise a special subset of the equations, the inverse transform can be found as follows: $g(t) = \int_\alpha^\beta f(a)k(\omega, t)da$. One of the widely used integral transforms is the Fourier transform. Abel transform is another one that has requirements for both of the functions. The Abel transform is widely applied for atmospheric profile retrievals using radio occultation observations [22]. The general transform can be defined as follows:

$$f(a) = \int_0^\infty g(r)k(r, a)dr \tag{2.36}$$

where

$$f(a) = \begin{cases} \frac{2r}{\sqrt{r^2-a^2}} & \text{if r} > \text{a} \\ 0 & \text{Otherwise} \end{cases}$$

or alternatively

$$f(a) = \int_0^\infty g(r)\frac{2r}{\sqrt{r^2 - a^2}}dr \tag{2.37}$$

In many applications the function f(a) is an abscissa function and g(r) is a radial function. The variables r and a represent a radius and an abscissa respectively. An inverse Abel transform exists in the form

$$g(r) = -\frac{1}{\pi}\int_r^\infty \frac{f'(a)}{\sqrt{a^2 - r^2}}da \tag{2.38}$$

For GPS RO usually g(r) is the electron density as a function of altitude and f(a) is the TEC measurement along the GPS-LEO ray.

2.3.2 Inversion Using Slant TEC Measurements

Inversions based on slant TEC measurements should assume that the LEO-GPS ray bending angle is very small. For the ionospheric F region altitude this assumption is valid. The

inversion based on slant TEC (STEC) is an onion-peeling method as illustrated in Figure 2.3. For electron density retrieval by CDAAC this method is used instead of using inversions from bending angle [22]. Total electron content (TEC) along the GPS-LEO ray can be expressed

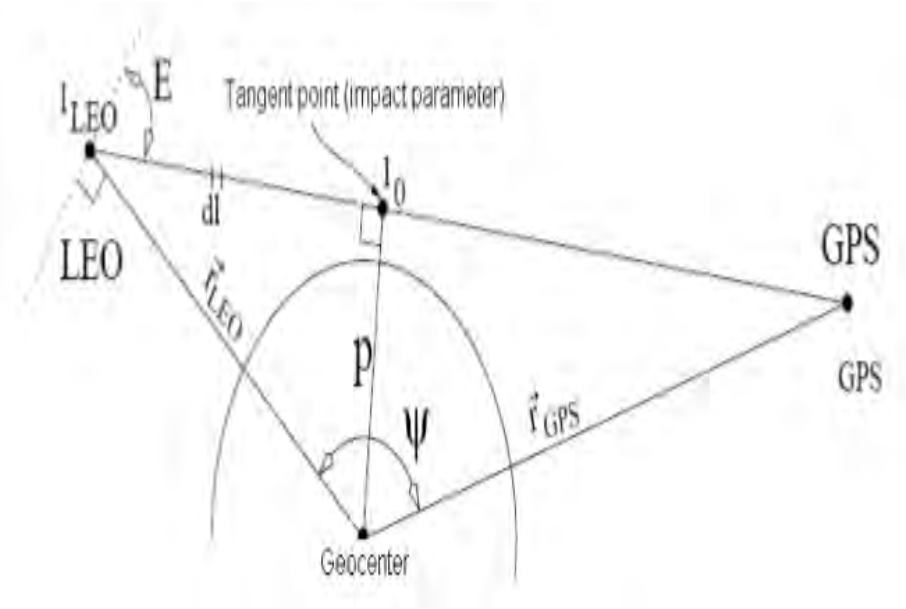

Figure 2.3: Illustration of occultation geometry with straight line GPS-LEO ray [after Garcia-Fernandez, 2002]

as follows.

$$TEC = \int N dl = -\frac{f^2}{40.3 \times 10^6} \int (n-1) dl = -\frac{f^2 S}{40.3} \tag{2.39}$$

where N is electron density, n is the ionospheric index of refractivity and S is the excess phase product (which is obtained directly from COSMIC data archives). TEC can be calculated from either L1 or L2 excess phase observations or from a linear combination of both:

$$TEC = -\frac{f_1^2 S_1}{40.3} = -\frac{f_2^2 S_2}{40.3} = \frac{1}{40} \left(\frac{1}{\frac{1}{f_2^2} - \frac{1}{f_1^2}} \right) (s_1 - s_2) \tag{2.40}$$

TEC computation from a single frequency observation contains effects of orbital motion and drifts of GPS transmitter and receiver clocks; these must be estimated through additional processing using ground reference data. For dual frequency TEC calculations the orbit and clock error are eliminated in formation of the dual-frequency linear combination - due to the fact that such errors are identical for L_1 and L_2 measurements. However in formation of the dual-frequency combination additional noise (primarily from L_2) will be introduced into TEC estimates. This error can be neglected in the future with improved civilian L_2 signals from GPS modernization efforts. TEC along the GPS-LEO link in Fig. 2.3 is expressed as

$$STEC = \left\{ \int_{l_0}^{l_{LEO}} + \int_{l_0}^{l_{GPS}} \right\} N_e(r) dl = \left\{ \int_{l_0}^{l_{LEO}} + \int_{l_0}^{l_{GPS}} \right\} \frac{N_e(r) r}{\sqrt{r^2 - p^2}} dr \tag{2.41}$$

where r is the altitude of LEO satellite and p is the tangent point altitude. Ne(r) is the electron density along the line of LEO-geocenter. With the assumption of spherical symmetry, STEC along the GPS-LEO ray is transformed into the density profiled along the LEO and geocenter

line. The electron density above the GPS satellite is also neglected in calculations. The spherical symmetry assumption will introduce error since the ionosphere can have large horizontal gradients within several kilometers as small ionospheric irregularity exists. It is assumed that STEC from tangent point of the GPS satellite is the same as STEC from tangent point to LEO in Figure 2.3 and expressed as

$$STEC = 2\int_{l_0}^{l_{LEO}} \frac{N_e(r)r}{\sqrt{r^2 - p^2}} dr \tag{2.42}$$

The Abel inversion is applied to this formulation and the relation between electron density and the calibrated STEC is given by

$$N_e(r) = -\frac{1}{\pi}\int_{r}^{r_{LEO}} \frac{dSTEC(p)/dp}{\sqrt{p^2 - r^2}} dp \tag{2.43}$$

where r is the radius of the earth, r_{LEO} is the distance from the geocenter to LEO satellite, p is the impact parameter and N_e is electron density.

Chapter 3

Ionospheric Tomography

In many applications, people feel need to examine the internal structure of an object with out opening it. Physician wants to see inside the human body and geologist yearn for a cross-section of the earth. For various reasons, they can not afforded to make many openings in the object. The ensemble of non-inverse techiniques to make these cross-section goes by the name Tomography. The word comes from greec noun $\tau o \mu \eta$, which means slice. All tomographic techiniques make use of waves. The waves can be electromagnetic or acoustic in origin. They can be emitted, absorbed, transmitted, reflected, refracted and diffracted or combinations of these, by structures inside the object. Therefore, we speak of emission, transmission, reflection and diffraction tomography. In all cases, waves from many propagation directions must be observed. The more viewing directions, the better the reconstruction of the object. In short, tomography images the internal structure by looking from many directions through the object [17].
Ionospheric tomography is a technique for remotely sensing electron density which is done by passing finite rays through the space of consideration and observing the spatial distribution of its physical quantity [23]. Ionospheric tomography is a two step process. First, integral measurements are made of them the medium of interest, ideally along many paths at many different viewing angles. Second, these integral measurements are inverted to obtain an estimate of the field. An ionospheric tomography has also two strengths relative to conventional in situ point measurements. First, as instruments are added, the amount of data goes up roughly quadratically: under ideal circumstances, the amount of data grows as the product of the number of sources and the number recivers. The second strength lies in the integral, path-averaging nature of the basic measurements [24].
And Yeh and Raymund investigated some of the theoretical limitations of ionospheric tomography. The geometry in LEO satellite-to-Earth configuration only allows observations over a limited number of viewing angles. In particular, the orientations of the satellite-to-receiver ray paths are biased in a vertical sense with no ray paths running horizontally through the ionosphere because of the curvature of the Earth. Consequently the vertical electron-concentration gradient is poorly defined by the TEC measurements alone. This geometrical constraint means that the reconstruction of the tomographic images is not straight forward and the reconstruction can not be implemented directly using conventional inversion algorithms alone. This fact has contributed towards making ionospheric imaging a challenging research topic, bringing together mathematicians, physicists and engineers [2].

3.1 Inverse Problem

Tomography is a part of the class of inverse problem, which is distinct from the class of direct problems. Both types of problems deals with state of an object on the one hand, and with a set of observation on the other. Of courese, the state of object and the outcomes of the experiment data are related by the laws of such that physics.
The direct prolem is a matter of explaination: given the state of the object, explain or predict the outcome of the expriment. This is the problem computational physicists are concerned with. The direct problems follows the natural order of the couse and effect.
The inverse problem is a matter of inference: what can we say about the state of an object from the observation or the experiment data? Here the order is reversed: deduce the couse from the effect. It is clear that the direct problem must be well understood, before attempts to solve the inverse problem can be made. In tomography, the unknown state is the two dimensional distribtuion and the experimental data corresponds to the line integrals.
In tomography, the inverse problem is equivalent to finding a solution to a set of integral equations. Another type of inverse problem need a solution to set of partial differential equations. In both cases physics determines the shape of the equations. The experimental data gives the values of the integral in the first case and the initial and boundary conditions in the latter [17].

3.2 Theory of Computrized Ionospheric Tomography (CIT)

The basic concept in CIT research is to use low-flying satellite as moving transmitters and arrays of reciver to measure TEC (Total Electron Content) in the ionosphere. Total electron content, TEC, is defined as the line integral of the electron density along a radio-wave propagation path from a satellite, S, to a receiver, R. The TEC may be expressed as

$$TEC(\beta, \chi_r) = \int_S^R N_e ds \tag{3.1}$$

where N_e = is the electron density;
β = elevation angle;
χ_r = location of receiver;
N_e = electron number density; and
S = arc link.
The TEC is obtained from the reciver Doppler data by estimating an unknown constant of intergation. By using an array of reciver and collecting data over a large angular apeture, the number density can be reconstructed from the data [25]. Assuming the electron density distribution to be stable during the selected time period, the image can be divided into sevral small pixel. Within each pixel, the electron density is assumed to be a constant, so the continuous density is assumed to be a constant, so the continuous density distribtuion N_e is discretized into n pixels, and the discretized distribtuion is represented by a column vector x [26]. The set of TEC measurements is expressed as a column vectory. In order to relate the discretized electron density distribtuion to the TEC measurements, a coffecient matrix A is introduced, so equation (3.1) can be given as

$$y_{n\times 1} = A_{m\times n} x_{n\times 1} + e_{n\times 1} \tag{3.2}$$

The element A_{ij}, which is the element in the i^{th} row and j^{th} column of A, corresponds to the length of the i^{th} ray path traversing the j^{th} pixel. m represent the number of ray paths,

and n expresses the number of pixels in probed region. In other words, each row of the matrix corresponds to a ray received at the given time and each column represents a pixel. e is a column of n values representing the error due to data noise and discretization. Hence, equation (3.2) can be simplified as

$$y_{n\times 1} = A_{m\times n} x_{n\times 1} \tag{3.3}$$

However, an inversion algorithm is required to determine the unknown electron density distribution from known y and A. The loss of information and inconsistency of data make ionosphere tomography an ill-posed inverse problem [27].

3.3 Tomography Algorithm

In order to resolve the ill-posed of ionospheric tomography, numereous algorithm have been presented in recent years. The Algebraic Reconstruction Technique (ART), the Multiplicative Algebraic Reconstruction Technique (MART) and Maximum Entropy Method (MEM) are some of the widely used of Computerized Ionospheric Tomography (CIT) algorithms. Raymund has made a comprative assessment of various CIT algorithms and observed that no single algorithm can be considered as the best. Some algorithm that construct well in one case can do verly poorly in other cases. It was also observed that the fundamental assumptions make significant differences and proper choice of algoritm will be the prime requisite for meaningfull data reconstruction [28]. But in this research, we use Tikhonov Regularization algorithm.

3.4 Tikhonove Regularization

Ionospheric tomography is a part of the family of ill-posed problem [28], which can be written in the form of a system of linear equation. A common way to solve equation (3.3) is to generate the estimated value of x as the least square solution to the set of equation.

$$x_{Ls} = arg_x min(||Ax - y||^2) \tag{3.4}$$

where $||.||$ denotes l_2 norm of a vector. when A is ill-conditioned, the least-square reconstructed object X_{ls} obtaind through equation (3.3) will be corrupted by amplified noise. There are many methods for regularizing such problems in order to generate reasonable estimate. Tikhonov regularization is one such method.

$$min_{x\in\Re^N}(||Ax - y||^2 + \alpha^2||Lx||^2) \tag{3.5}$$

where α is the regularization parameter and α >0, L is positive define matrix. L takes different forms in accordance with the order of regularization. For zero order Tikhonov regularization L=I, the identity matrix and for first order Tikhonov regularization:

$$L = \begin{pmatrix} -1 & 1 & 0 & . & . & 0 \\ 0 & -1 & 1 & 0 & . & 0 \\ . & . & . & . & . & . \\ . & . & . & . & . & . \\ 0 & . & . & 0 & -1 & 1 \end{pmatrix}$$

where L is a $P \times N$ matrix
Equation (4.1) can now be written as

$$min(|| \begin{pmatrix} A \\ \alpha L \end{pmatrix} x - \begin{pmatrix} y \\ 0 \end{pmatrix} ||^2) \tag{3.6}$$

The normal equation are

$$(A^T \alpha L^T) \begin{pmatrix} A \\ \alpha L \end{pmatrix} x = (A^T \alpha L^T) \begin{pmatrix} y \\ 0 \end{pmatrix} \tag{3.7}$$

Or

$$(A^T A + \alpha^2 L^T L)x = A^T y \tag{3.8}$$

The Tikhonov regularized solution can be written from above equation as

$$x_{\alpha.L} = (A^T A + \alpha^2 L^T L)^{-1} A^T y \tag{3.9}$$

The solution x is a function of the regularization parameter α, as well as L. The solution varies with regularization parameter quite strongly as compared to L.

Chapter 4

Result and Discussion

When the computerized ionospheric tomography technique is performed by using ground-based GPS data, the horizontal ray paths are usually absent due to the geometry of GPS ray path or due to the shape of the earth. However, the horizontal ray are very important to improve the vertical resolution of the reconstructed images. The absence of horizontal ray path often makes the vertical resolution of the inverted electron density profile very limited. In recent years, the risen of occultation can provide the horizontal ray paths needed by electron density reconstruction. To solve with the above limitation to some extent, COSMIC occultation observations are also used in this work. Using the Tikihonove Regularization algorithm, a series of iterative process is carried out to modify the electron density value inside the pixels crossed by the COSMIC-GPS and GPS-Ground reciver radio links. Chemical and dynamical processes are the reasons of electron density variation on the ionosphere. The chemical processes are the production and loss of the plasma, which is perdominat in the bottom side ionosphere. The major dynamical processes are the field aligned diffusion and the field perpendicular E×B drift due to the zonal electric field [29]. Relative importance of each processes varies with latitude and local time shown in Fig. 4.1 and Fig. 4.3. Fig. 4.1 shows the dirunal variation of electron density for January 1, 2008. A hight-versus-geographic latitude grid has been used. It can be seen from Fig. 4.1 that the variation of electron density for the day and night time. The ionization (enhancement) of elctron density is start to rising at 0500 UT and continue up to 1300 UT (Fig. 4.1c - Fig. 4.1g), with its maximum enhancement at 1300 UT (Fig. 4.1f) and start to fall at 1500 UT (Fig. 4.1h). The phenomena of rising and falling of the enhancement of the elelctron density is related to the rotation of of the Earth from west to east or resulting in day-night difference.

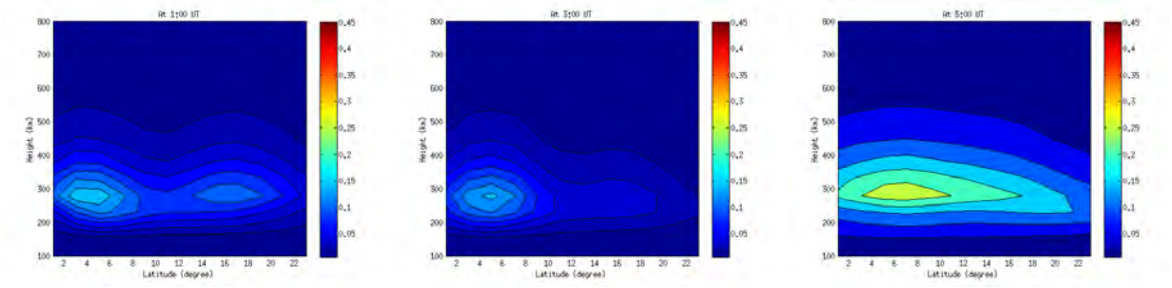

(a) (b) (c)

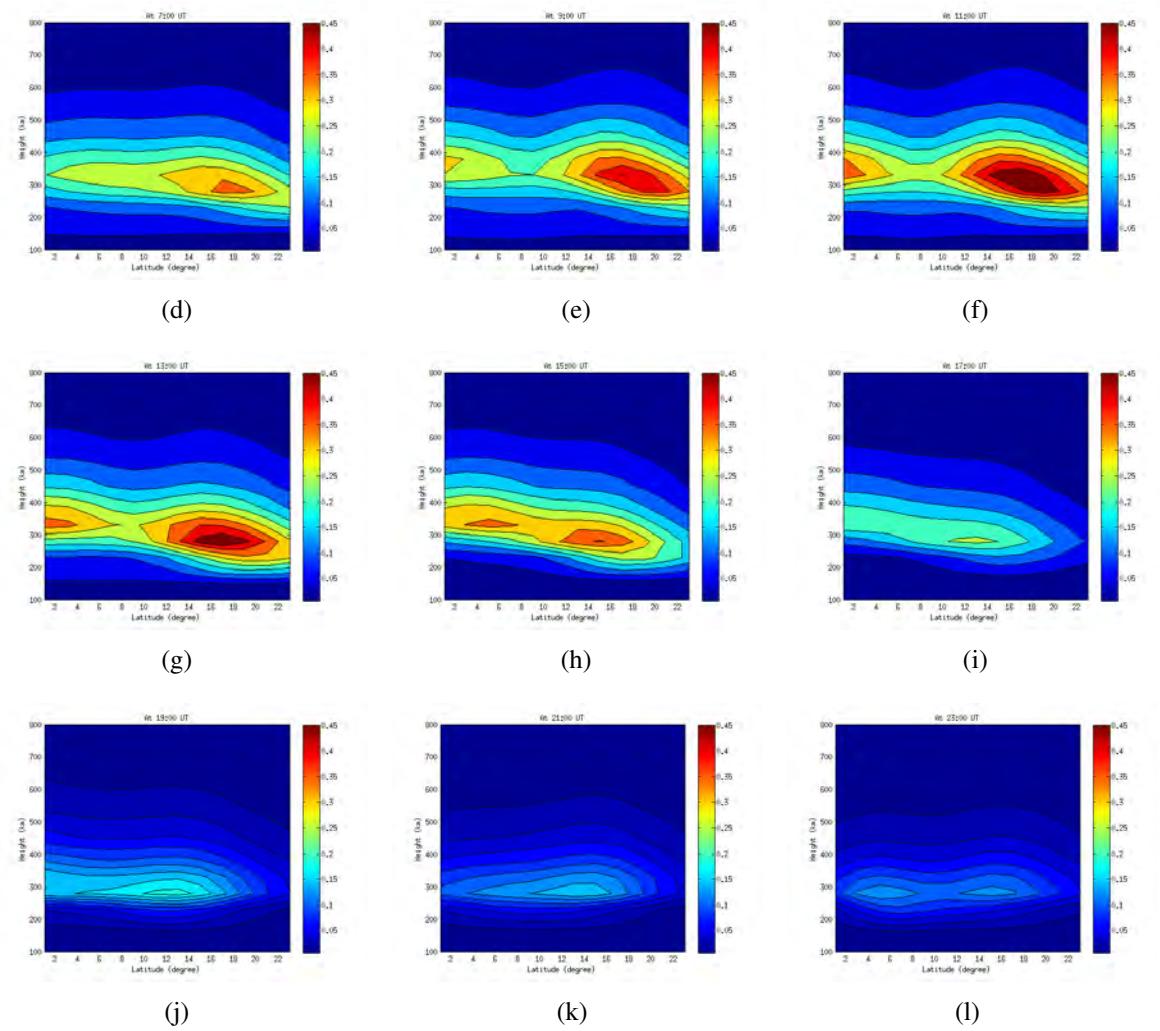

(d) (e) (f)

(g) (h) (i)

(j) (k) (l)

Figure 4.1: Durinal variation of reconstructed electron density at 38^0 geographic longitude for January 1, 2008. (The unit of the color bar is $10^{11}\ e/m^3$)

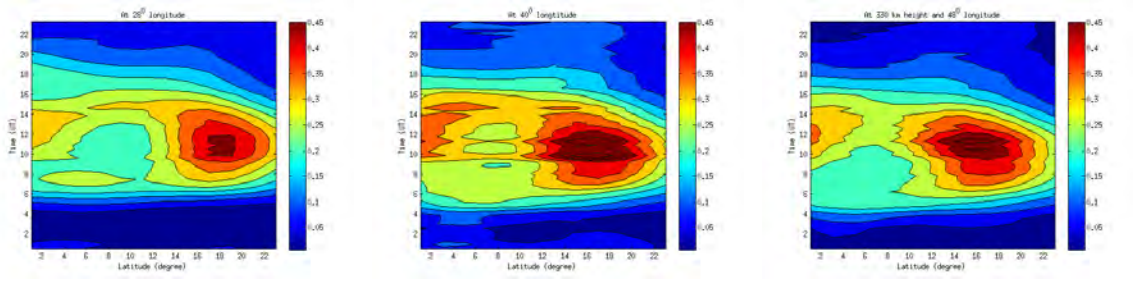

(a) (b) (c)

Figure 4.2: Reconstructed electron density at 3 different geographic longitude but at 330 km altitude for January 1, 2008. (The unit of the color bar is $10^{11}\ e/m^3$)

Fig. 4.2 shows latitude-time cross section for three different longitude. The peak electron density is achieved at approximately 10 UT for all longitude sectors. There is enhanced electron density over the eastern longtiude sector compared to the longitude sector towards western side or the study side region. Latitudinally, more electron density towards the north

with minimum electron density located within $5 - 11^0$N.

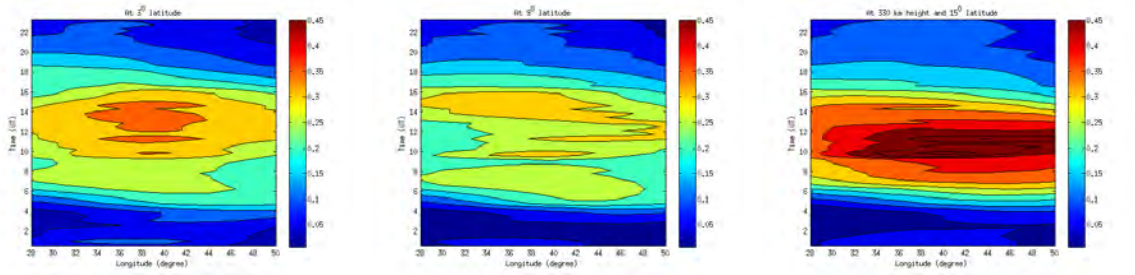

(a) (b) (c)

Figure 4.3: Reconstructed electron density at 3 different geographic latitude but at 330 km altitude for January 1, 2008. (The unit of the color bar is 10^{11} e/m^3)

Fig. 4.3 illustrates the latitudinal variation of electron density. As we go from the equator to both side of the latitudinal ionosphere up to the equatorial ionization anomaly the electron density value increases but in Fig. 4.3 we focuse only on the northen low latitude of the ionosphere. As shown in the figure, the electron density start to increase as the geographic latitude goes from 3^0-15^0N (Fig. 4.3a to Fig. 4.3c). This shows that there is a strong relation ship between the elctron density and geographic latitude due to position of the sun on the sky.

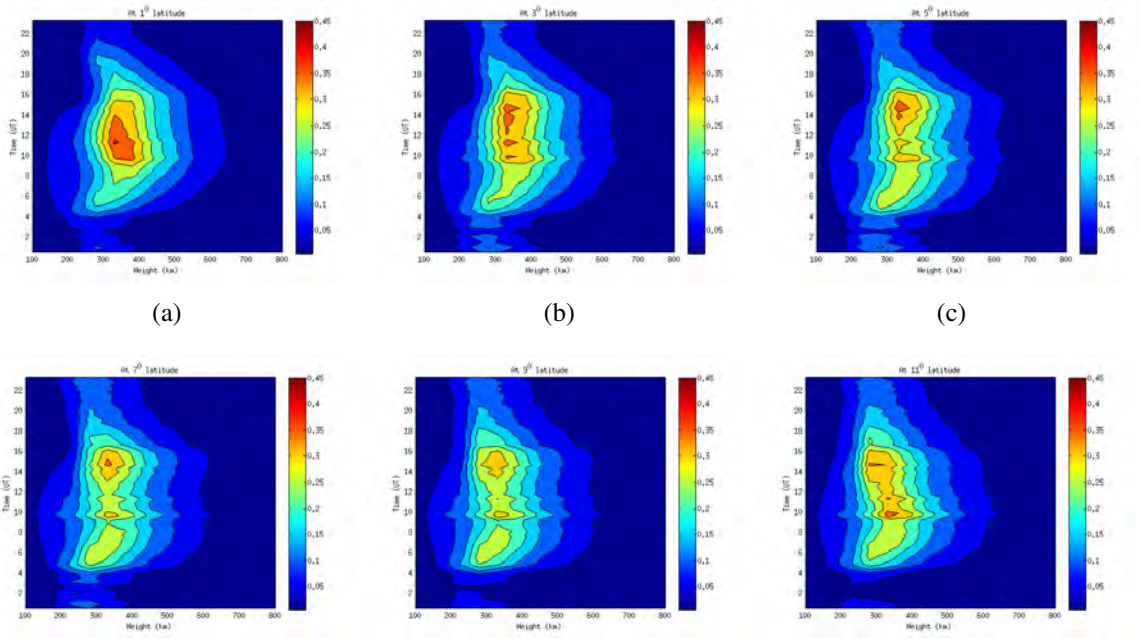

(a) (b) (c)

(d) (e) (f)

Fig. 4.4 indicates the variation of electron density for different low-latitude. As shown in the Fig. 4.4, as the latitude increase from around the equator to around 13^0 geographic latitude (Fig. 4.4a - 4.4g) the electron density do not vary much but starting 15^0 to 19^0 geographic latitudes (Fig. 4.4h - 4.4j) the electron density attains its maximam and start falling at 21^0N (Fig. 4.4l). This shows, the highest electron density is found at equatorial ionization anomaly. This high electron density is supposed to be at the equator but due to

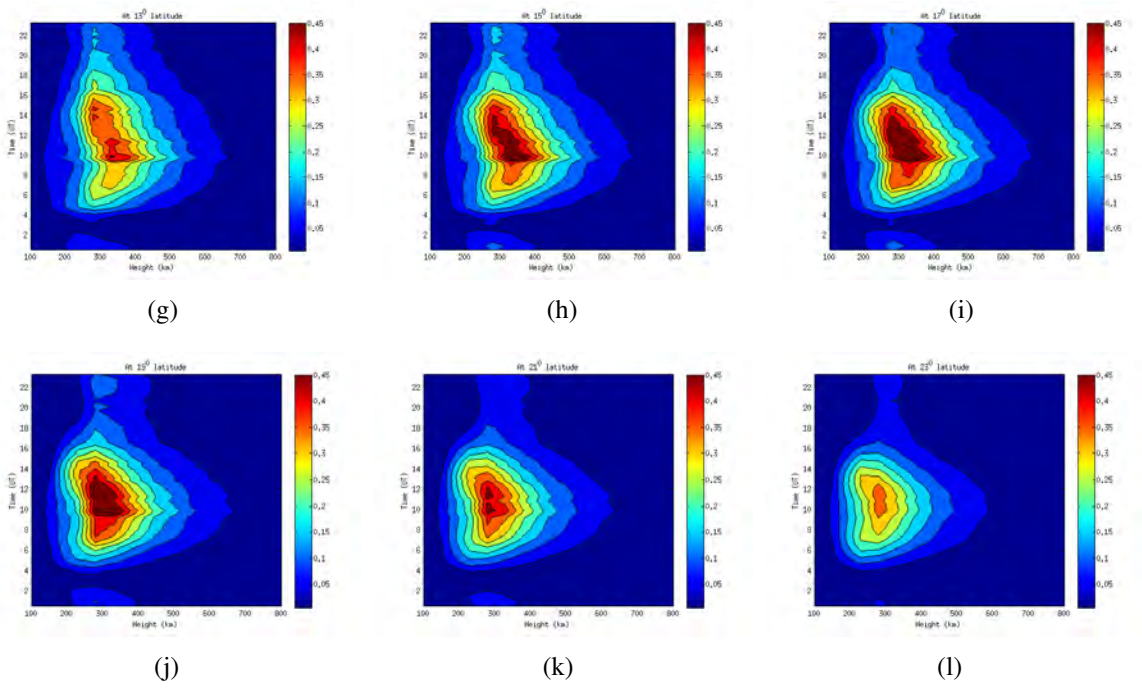

(g) (h) (i)

(j) (k) (l)

Figure 4.4: Reconstructed electron density at different geographic latitude but at 38^0 geographic longitude for January 1, 2008. (The unit of the color bar is $10^{11}\ e/m^3$)

the geometry of the magnetic field and the presence of the electric field, it is found at the equatorial ionization anomaly.

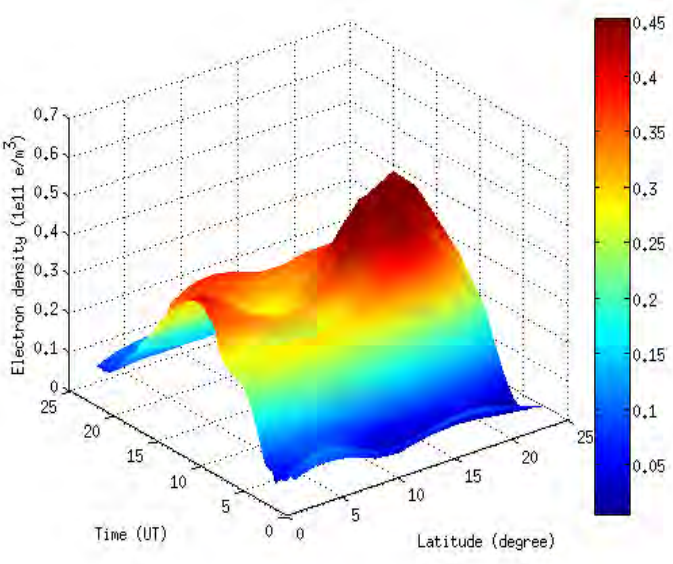

Figure 4.5: Reconstructed 3D plot electron density for 38^0 longitude at 330 km altitude for January 1, 2008. (The unit of the color bar is $10^{11}\ e/m^3$)

The 3D plot of the reconstructed electron density for 38^0 longitude at 330 km altitude to demonstarte the maximum and minimum value of the electron density is in Fig.4.5. As shown in the figure, the maximum and minimum electron density at 330 km altitude within this latitude range is $0.45 \times 10^{11} e/m^3$ and $0.1 \times 10^{11} e/m^3$ respectively. The electron density

start to increas around 0500 UT and reaches its EIA (Equatorial Ionization Anomaly) at around 1500 UT. This shows the ionization start around the morning and extended to its maximum value at after noon time. This agrees with the theory that states the day time have high electron density than night time.

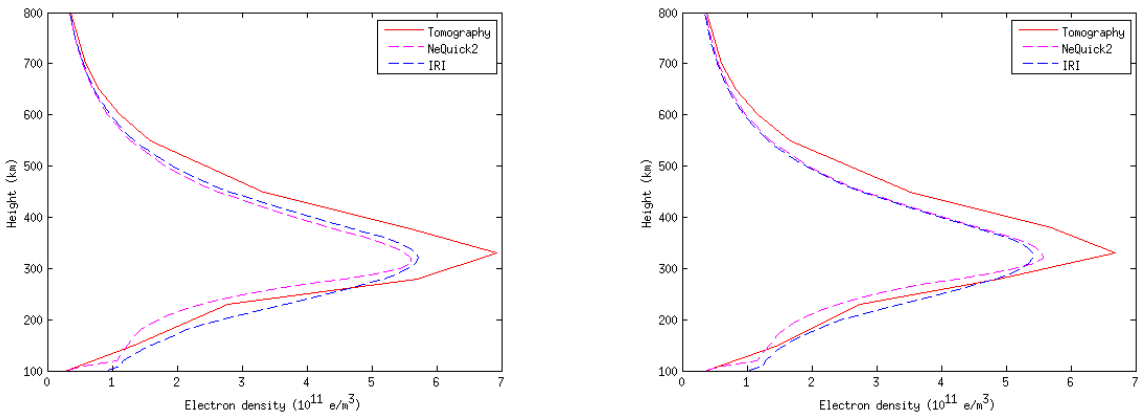

Figure 4.6: A comparison of the tomographically reconstructed electron density profiles with those obtained from both NeQuick2 and IRI models at 9^0 latitude and 38^0 longitude at 7:00 UT and at 11:00 UT for january 1.

Fig.4.6 shows the comparison of the reconstructed electron density profile with those obtained from both IRI 2007 and NeQuick2 models. NeQuick model electron density has been used as apriori in the tomographic inversion. The good agreement between NeQuick and reconstructed electron density is an indication that part of the reconstructed electron density is obtained from NeQuick model. However, the difference between NeQuick and reconstructed electron density at some latitude reveals that the information from GPS (ground-based) and COSMIC satellites helped in diclosing some features (variations) not captured by the model. The agreement between IRI and reconstructed electron density in the first panel of Fig. 4.6 by exhibiting maximum electron density at the same altitude is another indication that the tomography reconstruction has an added value despite sparse GPS network and COSMIC data used in this work.
Moreover, the different peak heights in the two models and reconstructed electron density in the right panel of Fig. 4.6 show that the role of the measurments from GPS and COSMIC satellites in revealng new feature than that deprcted by the two climatological models. Therefore, the difference between the models and tomographical reconstructed electron density, indeed, show the strength of inversion than its weakness. The appropriate of the derived electron density should be evaluated by considering its agreement with theory.

Chapter 5

Conclusions

This work is intended to test the algorithm to combine GPS STEC and COSMIC STEC in tomography reconstruction of electron density over East Africa longitude sector. A network of ground-based GPS recivers between 10-15 and COSMIC observatons over the region are used in the reconstruction. Since this network is very sparse, apriori information on electron density is provided by NeQuick model. The reconstructed electron density is, therefore, a weighted average of this aprrori electron density from NeQuick and that of the measurements from ground-GPS and COSMIC satellites. The accuracy and appropriateness of the reconstructed electron density are evaluated by comparison with IRI and NeQuick models. The soundness of the results is also assessed through investigation of diurnal, longitudinal and latitudinal variations. The results are consistent with what would have been suggested by the physics operating in the ionosphere. The reconstructed electron density attains its peak over the climatologically expected EIA region. The minimum electron density is also observed near the equatorial region. The peak electron density altitude is located between 300-400 km as expected which varies with time of observation consistent with ionospheric physics. As this work is a case study to investigate the robustness of the employed algorithm, complete study of the ionosphere has to be done with observations that consists of longer periods, typically over a year or more, to understand the electron density distribution and variability.

Bibliography

[1] Endawoke Yizengaw, Peter Dyson, and Elizabeth Essex, "Tomographic reconstruction of the ionosphere using ground-based GPS data in the Australian region", Physics department, La Trobe university, Bundoora, Vic 3086, Australia.

[2] Bust, G.S.; Mitchell, C.N.,"Review of the current status of Four-Dimensional Ionospheric Imaging", In characterising the ionosphere (PP.31-1-31-18). Meeting proceedings RTO-MP-IST-056, paper 31. Nevilly -Sur-Seine, France, 2006.

[3] Attila Komjat, "Global ionospheric total electron content mapping using the Global Positioning System ", PhD. Dessertation, Department of Geodesy and Geomatics Engineering, University of New Brunswick, Canada, September 1997.

[4] Xiao Dongyuan, Hun Mingo, "Study of low-latitude ionospheric irrgularity structure based on a new LTIN ", PhD. Dessertation, National central University space science research institute, China, 1997.

[5] Zama Thobeka Katamzi, "Stastical analysis of ionospheric total electron content", PhD. Dessertation, Department of Electronic and Eletrical Engineering, University of Bath, March 2011.

[6] Bdl Opperman," Reconstructing ionospheric TEC over South Africa using signals from a regional GPS network", PhD. Dessertation, Rhodes University, 28 November 2007.

[7] Tamas I.Gombosi, "Physics of the space environment", The pitt building, Trumpington street, Cambridge, United King dom, ISBN 0 521 59264 x, ISBN 0 521 60768 x, 1998.

[8] Mark Moldwin, "An introduction to space weather", New York, USA, ISBN-13 978-0-511-39304-4, ISBN-13 978-0-521-86149-6, 2008.

[9] Margaret G.Kivelson, Christopher T. Russell, "Introduction to space physics", 40 west 20th street, New York, NY 10011-4211, USA, ISBN 0-521-45104-3, ISBN 0-521-45714-9, 1995.

[10] B.S. Dandekar, J.Buchu, J.A. Whalen, P. Fougere, "Physics of the ionosphere for OTH operation", PL-TR-95-2149, Environmental research papers, No.1183.

[11] Thomas F.Tascione, "Introduction to the space environment", second edition, Orbit book company, INC., Malabar, Florida 329570, ISBN 0-89464-009-7, ISBN 0-89464-020-8, 2005.

[12] Robert W.Schunk and Andrew F.Nagy, "Ionospheric physics, plasma physics and chemistry", Second edition, New York, USA, ISBN-13 978-0-511-63489-5, ISBN-13 978-0-521-87706-0, 2000, 2009.

[13] Dave Anderson and Tim Fuller-Rowell, "Space environment", Space environment center, 325 broad way, Boulder, Co 80303-3326, SE-14, 1999.

[14] R.Bent, "Bent ionospheric model", DBA system inc., Melbourne, Florida 32901, 1972.

[15] R.E. Daniell, L.D. Brown, D.N. Anderson, M.W. Fox, P.H. Dohorty, D.T. Decker, J.J. Sojka, and R.W. Schunk,"Parameterzed ionospheric model: A Global ionospheric parametrization based on the first principle mode", Radio science, 30, 5, 1499-1510, 1995.

[16] http://t-ict4d.ictp.it/nequick2.

[17] Gijsbert Christian Fehmers, "Tomography of the ionosphere", Department of physics, Eindoven university of technology, Netherland, ISBN 90-386-0438-6.

[18] C.Rocken, Y-H. Kuo, W. Schreiner, D. Hunt, S. Sokolovskiy, "COSMIC system description", Special issue of terrestrial, Atmospheric and Ocean science, 11(1), 21-52, March 2000.

[19] Dao Ngoc Hanh Tam, "Global comparisons of NmF_2 and hmF_2 between COSMIC and ionosondes", Master thesis, Taiwan, June 2010.

[20] M.J Angling, "First assimilation of COSMIC radio occultation data into the Electron Density Assimilative Model (EDAM)", Ann. Geophys, 26, 353-359, 2008.

[21] Gebreab Kidanu, "Tomographic Imaging of Ionospheric Electron Density over Ethiopia using Ground based GPS receivers", Addis Ababa University, Physics Department, June 2012.

[22] Man Feng, "Detection of high-latitude ionospheric irregularity from GPS radio occultation", Master thesis, Department of Geomatics Engineering, Schulich school of Engineering, Calgary, Alberta, May 2010.

[23] Sukanta Kumar Das, Ashish Kumar Shukla, "Two-dimensional ionospheric tomography over the low-latitude indian region: An inter comparison of ART and MART algorithms", radio science, vol.46, Rs 2005, doi:10.1029/2010 Rs 00 4350, 2011.

[24] Zhizho Liu and Yang Gao, "Ionospheric tomography using Gps measurements", Department of Geomatics Engineering, The university of Calgary, Calgary, Alberta Canada T2N 1N4.

[25] Arnold J. Tucker, “Computerized ionospheric tomography”, Johns Hopkins APL technical digest, Volum 19, number 1(1998).

[26] Debo Wen, Sanzhi, Pingying Tag, “Tomographic reconstruction of ionospheric electron density based on constrained algebraic reconstruction technique”, GPS solut, 14:375-380, doi:10.1007/5 10291-010-0161-0, 2010.

[27] K. Bhuyan, S.B. singh and P.K. Bhuyan, “Tomographic reconstruction of the ionosphere using generalized singular value decomposition”, current science, Vol.76, No.7, 10 April 1999.

[28] K. Bhuyan, S.B. singh and P.K. Bhuyan, “Application of generalized singular value decomposition to ionospheric tomography”, Annales Geophysical, 22:3437-3444, SRef-ID:1432-0576/ag/ 2004 - 22 - 3437, 2004.

[29] Takashi Maruyama, “Longitudinal Peculiarity of topside electron density at 1100 km”, communication research laboratory, 2-1 Nukuikita 4-chomo, Koganei, Tokyo, 184-8795 Japan.